been reported in many human disorders, and these have been used for disease diagnosis and for the elucidation of disease pathomechanisms [4, 8]. Focusing on glycoproteins *N*-glycans, it was demonstrated that the mouse epidermis had abundant high-mannose oligosaccharides [24]. In addition, the oligosaccharide-binding proteins were also determined [24]. However, there are no reports of studies on *N*-glycans in human epidermis. In the present study, we studied *N*-glycan profiles in normal human epidermis and the stratum corneum of ichthyotic, hyperkeratotic skin. *N*-Glycans were specifically released by *N*-glycosidase F and were labeled by pyridylamination with a fluorescence tag. Oligosaccharide profiles were analyzed using high-performance liquid chromatography (HPLC) [10, 22].

Skin samples of normal, non-hyperkeratotic epidermis were collected from control non-palmoplantar skin of three patients with benign skin tumors at resection operations. Skin scale samples were collected from hyperkeratotic skin from the legs of five ichthyosis patients, three non-bullous congenital ichthyosiform erythroderma patients and two lamellar ichthyosis patients. The medical ethical committee at Hokkaido University approved all the described studies. All the participants or parents of the participants gave their written informed consent.

Skin scales were collected by gently scraping the patients' legs with a dull scalpel and stored at −70°C. Normal epidermal samples were obtained at resection operations of benign subcutaneous tumors after obtaining fully informed consent from the patients. Samples from both the ichthyosis patients and normal healthy controls were stored at −70°C.

Normal skin samples were heated to 60°C for 1 min in phosphate buffered saline (PBS) and then cooled on ice. The epidermis was stripped off with a scalpel and was used for further analysis. The epidermis of normal skin samples was washed three times in PBS. Both the scales and the separated epidermis were denatured at 90°C for 10 min in 100 mM NH_4HCO_3 and then finely shredded with scissors.

To degrease the samples, each sample was put into a mixture of chloroform and methanol 2:1 (v/v) 600 µl, mixed well and centrifuged at 3,500 rpm, 4°C for 10 min. Then, the lower layer was removed. This procedure was repeated twice to remove lipids. Organic solvents in the upper layer were vaporized with nitrogen flow at 80°C and the aqueous solution dried in a centrifugal evaporator.

For trypsin and chymotrypsin digestion, the dried samples were suspended in 5 mg per 100 µl of 45 mM Tris–HCl buffer pH 8 containing 10 mM $CaCl_2$, and 0.1 mg trypsin and 0.1 mg chymotrypsin (Sigma-Aldrich Japan, Tokyo, Japan) were added in a 1.5-ml microcentrifuge tube (Eppendorf type). The pH of the solutions was confirmed to be between 7 and 8 by the pH test paper. Toluene was added to the surface of the sample solution and kept at 37°C overnight in an incubator.

For *N*-glycosidase F digestion, trypsin and chymotrypsin were deactivated by heating sample tubes at 90°C for 10 min in a heat block. *N*-Glycosidase F (Roche Diagnostics, Tokyo, Japan) was added, 10 U for each 5 mg sample. The pH of the sample solutions was again confirmed and toluene was added. The samples were kept at 37°C overnight.

Pronase (0.1 mg, Calbiochem, San Diego, CA, USA) was added to each 5 mg of the sample for pronase digestion. pH of the sample solutions was checked again and toluene was added. The samples were incubated at 37°C overnight. After incubation, pronase was deactivated at 90°C for 10 min.

The oligosaccharide fraction was purified by gel-filtration on Bio-gel P-4 (Bio-Rad Laboratories, Hercules, CA, USA) column (1.0 cm × 38 cm) using water as an eluate, and lyophilized completely. The carbohydrates were reductively aminated with 2-aminopyridine and sodium cyanoborohydride [10, 29]. Pyridylaminated (PA)-oligosaccharides were separated from excess reagents by another gel-filtration column step using Sephadex G-15 (GE Healthcare Bioscience Corp., Piscataway, NJ, USA) and 10 mM NH_4HCO_3 and lyophilized again.

Each PA-oligosaccharide was dissolved in 100 µl of 0.01 N HCl and the pH was adjusted to 2 with 0.1 N HCl checking by test paper. PA-oligosaccharide solutions were heated at 90°C for 60 min to remove sialic acids and neutralized with 100 µl of 1 M NH_4HCO_3.

Each PA-oligosaccharide solution was purified by HPLC on an amide–silica column (TSKgel Amide-80 4.6 mm × 250 mm, Tosoh Corporation, Tokyo, Japan) using two solvents, A and B, at a flow rate of 1.0 ml/min at 40°C. Solvent A comprised 65% (v/v) of acetonitrile and 35% of 0.5 M acetic acid–triethylamine buffer pH 7.3 and solvent B was 35 and 65%, respectively. The column was equilibrated only with solvent A and 7 min after injection of each sample, the flow was changed to solvent B only. The *N*-glycan fraction that eluted between 8 and 12 min was collected and centrifugally evaporated.

Each oligosaccharide mixture was dissolved in water and analyzed by HPLC using the previously described procedure [22]. The PA-oligosaccharide mixture was applied on an ODS column (HRC-ODS 6 mm × 150 mm, Shimadzu Corporation, Kyoto, Japan). The

column was equilibrated with 0.1% (v/v) 1-butanol in 10 mM sodium phosphate buffer pH 3.8 and concentration of 1-butanol was linearly increased to 0.25% in 60 min. The flow rate was 1.0 ml/min and the column was controlled at 55°C. PA-glycans were detected by fluorescence, excitation at 320 nm and emission at 400 nm.

N-Glycan profiles from the patients and normal control epidermis are shown in Fig. 1 as chromatograms on an ODS column. *N*-Glycan eluted after 5 min and few contamination peaks were detected in this region. High-mannose type *N*-glycans eluted from 5 to 10 min and complex-type and hybrid-type *N*-glycans appeared at 10 min or later in this analysis. Three peaks, a, b and c, eluted at 15.8, 18.8 and 26.9 min, respectively, and these profiles were significantly altered in ichthyotic skin. The rates of these peaks are shown in Fig. 2. Peak c significantly decreased and peak b increased in the ichthyotic skin compared with normal controls. Peak a was also larger in the patients, but the statistical change in this level was not significant. Using two-dimensional mapping [22], peaks a, b and c to corresponded to major serum *N*-glycans, Galβ1,4GlcNAcβ1,2Manα1, 3(Galβ1,4GlcNAcβ1,2Manα1,6)Manβ1,4GlcNAcβ1,4 GlcNAc,Galβ1,4GlcNAcβ1,2Manα1,3(Manα1,6)Man β1,4GlcNAcβ1,4(Fucα1,6)GlcNAc and Galβ1,4GlcN Acβ1,2Manα1,3(Galβ1,4GlcNAcβ1,2Manα1,6)Manβ 1,4GlcNAcβ1,4(Fucα1,6)GlcNAc, respectively [17, 22].

Changes in *N*-glycan oligosaccharides have mainly been reported in carcinomas in the course of progression or during metastatic change [13, 14, 23]. In the epidermis, glycoconjugate profile changes were studied by lectin histochemistry in a variety of skin diseases [1, 2, 9]. In several autoimmune skin diseases, autoantibody targets have been shown to be *N*-linked oligosaccharides [18]. However, to our knowledge, this is the

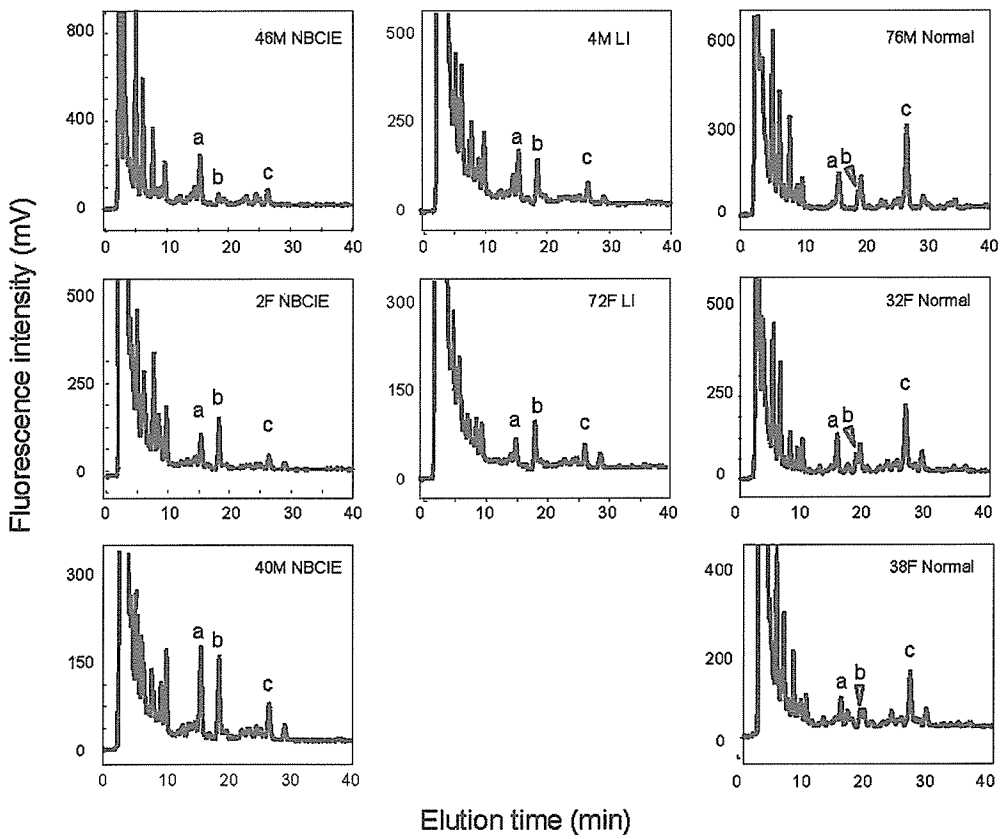

Fig. 1 Chromatograms of *N*-glycans from the epidermis. Fluorescence-tagged glycans released from the epidermis of patients and normal controls on an ODS column using HPLC. Peaks *a*, *b* and *c* correspond to *N*-glycans, Galβ1,4GlcNAcβ1,2Manα1,3 (Galβ1,4GlcNAcβ1,2Manα1,6)Manβ1,4GlcNAcβ1,4GlcNAc,Gal β1,4GlcNAcβ1,2Manα1,3(Manα1,6)Manβ1,4GlcNAcβ1,4(Fucα1, 6)GlcNAc and Galβ1,4GlcNAcβ1,2Manα1,3(Galβ1,4GlcNAcβ1, 2Manα1,6)Manβ1,4GlcNAcβ1,4(Fucα1,6)GlcNAc, respectively. *LI* lamellar ichthyosis, *NBCIE* non-bullons congenital ichthyosiform erythroderma

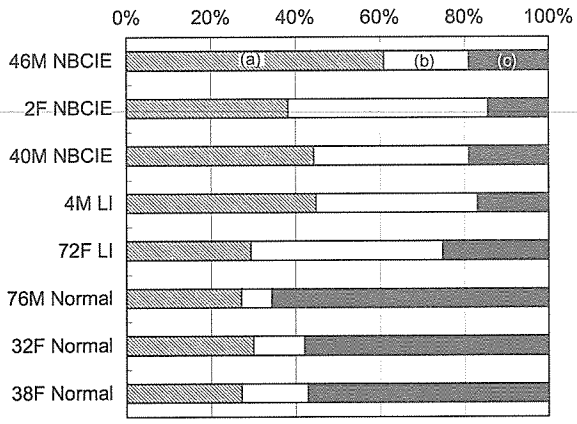

Fig. 2 Rates of molecular compartments, *a*, *b* and *c*. Compartments *a* and *b* were increased and compartment *c* decreased in the hyperkeratotic diseased skin from patients. Colors of *bar* show following: slashed, a; white, b; black c; *LI* lamellar ichthyosis, *NBCIE* non-bullons congenital ichthyosiform erythroderma

first study that reported *N*-linked oligosaccharide profiles in normal and hyperkeratotic epidermis.

Glycosylation is the major post-translational modification of many proteins. The *N*-Glycan precursor, Glc3Man9GlcNAc2, is introduced to asparagine residues of Asn-X-Ser/Thr sequence while polypeptide synthesis occurs in the endoplasmic reticulum. The Glc residues are removed while protein holding occurs. High-mannose type *N*-glycans work as a tag in the transfer of a protein folded correctly to the Golgi apparatus or misfolded one to degradation system [11]. In the Golgi apparatus, several enzymes modify *N*-glycan oligosaccharides from the high-mannose type into a more complex type by trimming and repetitive addition of sugar residues [15]. The biosynthesis of *N*-glycans is highly conserved and these oligosaccharide residues on proteins have important roles in promoting protein regulation, folding, quality control, sorting and transport [6].

The *N*-glycan alterations seen in ichthyotic skin failed to suggest novel oligosaccharide structures, although the rates of known oligosaccharide structures were changed. Peak a is the most common *N*-glycan in the human serum. Peak b is formed due to insufficient activity of *N*-acetylglucosaminyltransferase II (GnT-II) and peak c is produced from peak a *N*-glycan by fucosyltransferase 8 (Fut8) activity [6]. The GnT-II knock-out mice were reported to die from serious defects of multiple organs in early postnatal development, mainly from abnormalities in the gastrointestinal tracts, hematopoietic systems and bones, although skin involvements were not apparent [26]. The Fut8 null mice were also lethal in early postnatal days mainly from emphysema-like changes in the lung [27]. The Fut8 null mice were known to overexpress matrix metaloproteinases and to show function loss of TGF-β receptor. TGF-β mediates a variety of signaling pathways [16] and dysfunction of TGF-β receptor may be associated with skin symptoms of ichthyosis in the present study. On the other hand, there is a possibility that disturbed differentiation of epidermal keratinocytes resulted in the altered *N*-glycan profiles in the ichthyotic lesions. In any case, the relationship between *N*-glycan alteration and hyperkeratosis is an interesting finding that may help to clarify the pathomechanism(s) of hyperkeratosis.

Epidermal proteins, which comprise high levels of mannose-type oligosaccharides, were analyzed in mouse [24]. These high-mannose type oligosaccharides are located in lysosomes, lamellar granules and cell–cell connection desmosome sites. Desmocollins and desmogleins are also assigned as carriers of high-mannose type oligosaccharides, and it was suggested that high-mannose type oligosaccharides control desquamation [24]. However, in the present samples of hyperkeratotic skin, the profile of the high-mannose type oligosaccharides was not changed. These results indicated that *N*-glycans bound to cell surface proteins were more seriously affected than those in the cytoplasm and desmosomes. Further studies into *N*-glycan structures and the respective proteins carrying the *N*-glycans in hyperkeratotic skin will provide further clues to determine the exact mechanisms that lead to hyperkeratosis in human skin.

Acknowledgments The authors thank Ms Mayuko Nagasaki for her excellent technical assistance. This work was partly supported by a grant for the National Project on "Functional Glycoconjugate Research Aimed at Developing New Industry" from the Ministry of Education, Science, Sport and Culture of Japan.

References

1. Akiyama M, Hayakawa K, Watanabe Y, Nishikawa T (1990) Lectin-binding sites in clear cell acanthoma. J Cutan Pathol 17:197–201
2. Akiyama M, Sugiura M, Shimizu H, Nishikawa T (1991) No significant change of glycoconjugates exists in the epidermis of familial benign chronic pemphigus. Arch Dermatol Res 283:537–539
3. Bell CM, Skerrow CJ (1984) Factors affecting the binding of lectins to normal human skin. Br J Dermatol 111:517–526
4. Butler M, Quelhas D, Critchley AJ, Carchon H, Hebestreit HF, Hibbert RG, Vilarinho L, Teles E, Matthijs G, Schollen E, Argibay P, Harvey DJ, Dwek RA, Jaeken J, Rudd PM (2003) Detailed glycan analysis of serum glycoproteins of patients with congenital disorders of glycosylation indicates the specific defective glycan processing step and provides an insight into pathogenesis. Glycobiology 13:601–622

5. Dabelsteen E, Buschard K, Hakomori S-I, Young WW (1989) Pattern of distribution of blood group antigens on human epidermal cells during maturation. J Invest Dermatol 82:13–17
6. Dwek RA (1996) Glycobiology: toward understanding the function of sugars. Chem Rev 96:683–720
7. Elias PM, Chung JC, Orozco-Topete R, Nemanic MK (1983) Membrane glycoconjugate visualization and biosynthesis in normal and retinoid-treated epidermis. J Invest Dermatol 81:81s–85s
8. Fukuda MN, Dell A, Scartezzini P (1987) Primary defect of congenital dyserythropoietic anemia type II. J Biol Chem 262:7195–7206
9. Gheri G, Russo G, Cappugi P, Sgambati E, Bryk SG (1999) The oligosaccharidic component of the glycoconjugates in lichen planus, granuloma annulare, seborrheic keratosis and plamoplantar keratoderma: lectin histochemical study. Histol Histopathol 14:697–704
10. Hase S, Ikenaka T, Matsushima Y (1978) Structure analyses of oligosaccharides by tagging of the reducing end sugars with a fluorescent compound. Biochem Biophys Res Commun 85:257–263
11. Helenius A, Aebi M (2001) Intracellular functions of *N*-linked glycans. Science 291:2364–2369
12. Helenius A, Aebi M (2004) Role of *N*-linked glycans in the endoplasmic reticulum. Annu Rev Biochem 73:1019–1049
13. Ishimura H, Takahashi T, Nakagawa H, Nishimura S-I, Hagisawa S, Arai Y, Horikawa Y, Habuchi T, Miyoshi E, Ohyama C (2006) *N*-Acetylglucosaminyltransferase-V (GnT-V) and β 1,6 branching *N*-linked oligosaccharides are associated with good prognosis of the patients with bladder cancer. Clin Cancer Res 102:15791–15796
14. Jorgensen T, Berner A, Kaalhus O, Tveter KJ, Danielsen HE, Bryne M (1995) Up-regulation of the oligosaccharide sialyl LewisX: a new prognostic parameter in metastatic prostate cancer. Cancer Res 55:1817–1819
15. Kornfeld R, Kornfeld S (1985) Assembly of asparagine-linked oligosaccharides. Annu Rev Biochem 54:631–664
16. Massagué J, Blain SW, Lo RS (2000) TGFβ signaling in growth control, cancer, and heritable disorders. Cell 103:295–309
17. Nakagawa H, Kawamura Y, Kato K, Shimada I, Arata Y, Takahashi N (1995) Identification of neutral and sialyl *N*-linked oligosaccharide structures from human serum glycoproteins using three kinds of high-performance liquid chromatography. Anal Biochem 226:130–138
18. Shimanovich I, Hirako Y, Sitaru C, Hashimoto T, Brocker EB, Butt E, Zillikens D (2003) The autoantigen of anti-p200 pemphigoid is an acidic noncollagenous *N*-linked glycoprotein of the cutaneous basement membrane. J Invest Dermatol 121:1402–1408
19. Skerrow CJ, Clelland DG, Skerrow D (1989) Changes to desmosomal antigens and lectin-binding sites during differentiation in normal human epidermis: a quantitative ultrastructural study. J Cell Sci 92:667–677
20. Srikrishna G, Varki NM, Newell PC, Varki A, Freeze HH (1997) An IgG monoclonal antibody against *Dictyostelium discoideum* glycoproteins specifically recognizes Fucα1,6GlcNAcβ in the core of *N*-linked glycans. J Biol Chem 272:25743–25752
21. Symington FW, Holmes EH, Symington BE (1992) Human epidermal keratinocyte expression of sialyl-Lewis X. J Invest Dermatol 99:601–607
22. Tomiya N, Awaya J, Kurono M, Endo S, Arata Y, Takahashi N (1988) Analyses of *N*-linked oligosaccharides using a two-dimensional mapping technique. Anal Biochem 1715:73–90
23. Tsuchiya N, Yamanaka R, Yajima N, Homma J, Sano M, Komata T, Ikeda T, Fujimoto I, Takahashi H, Tanaka R, Ikenaka K (2005) Isolation and characterization of an *N*-linked oligosaccharide that is increased in glioblastoma tissue and cell lines. Int J Oncol 27:1231–1239
24. Uematsu R, Furukawa J-I, Nakagawa H, Shinohara Y, Deguchi K, Monde K, Nishimura S-I (2005) High throughput quantitative glycomics and glycoform-focused proteomics of murine dermis and epidermis. Mol Cell Proteomics 4:1977–1989
25. Virtanen I, Kariniemi A-L, Holthöfer H, Lehto VP (1986) Fluorochrome-coupled lectins reveal distinct cellular domains in human epidermis. J Histochem Cytochem 34:307–315
26. Wang Y, Tan J, Sutton-Smith M, Ditto D, Panico M, Campbell RM, Varki NM, Long JM, Jaeken J, Levinson SR, Wynshaw-Boris A, Morris HR, Le D, Dell A, Schachter H, Marth JD (2001) Modeling human congenital disorder of glycosylation type IIa in the mouse: conservation of asparagine-linked glycan-dependent functions in mammalian physiology and insights into disease pathogenesis. Glycobiology 11:1051–1070
27. Wang X, Inoue S, Gu J, Miyoshi E, Noda K, Li W, Mizuno-Horikawa Y, Nakano M, Asahi M, Takahashi M, Uozumi N, Ihara S, Lee SH, Ikeda Y, Yamaguchi Y, Aze Y, Tomiyama Y, Fujii J, Suzuki K, Kondo A, Shapiro SD, Lopez-Otin C, Kuwaki T, Okabe M, Honke K, Taniguchi N (2005) Dysregulation of TGF-beta1 receptor activation leads to abnormal lung development and emphysema-like phenotype in core fucose-deficient mice. Proc Natl Acad Soc USA 102:15791–15796
28. Watt FM (1983) Involucrin and other markers of keratinocyte terminal differentiation. J Invest Dermatol 81:100s–103s
29. Yamamoto S, Hase S, Fukuda S, Sano O, Ikenaka T (1989) Structures of the sugar chain of interferon-γ produced by human myelomonocyte cell line HBL-38. J Biochem 105:547–555

ABSTRACT: Epidermolysis bullosa simplex with muscular dystrophy (EBS-MD, MIM 226670) is caused by plectin defects. We performed mutational analysis and immunohistochemistry using EBS-MD (n = 3 cases) and control skeletal muscle to determine pathogenesis. Mutational analysis revealed a novel homozygous plectin-exon32 rod domain mutation (R2465X). All plectin/HD1-121 antibodies stained the control skeletal muscle membrane. However, plectin antibodies stained the cytoplasm of type II control muscle fibers (as confirmed by ATPase staining), whereas HD1-121 stained the cytoplasm of type I fibers. EBS-MD samples lacked membrane (n = 3) but retained cytoplasmic HD1-121 (n = 1) and plectin staining in type II fibers (n = 3). Ultrastructurally, EBS-MD demonstrated widening and vacuolization adjacent to the membrane and disorganization of Z-lines (n = 2 of 3) compared to controls (n = 5). Control muscle immunogold labeling colocalized plectin and desmin to filamentous bridges between Z-lines and the membrane that were disrupted in EBS-MD muscle. We conclude that fiber-specific plectin expression is associated with the desmin-cytoskeleton, Z-lines, and crucially myocyte membrane linkage, analogous to hemidesmosomes in skin.

Muscle Nerve **35:** 24–35, 2007

PLECTIN DEFECTS IN EPIDERMOLYSIS BULLOSA SIMPLEX WITH MUSCULAR DYSTROPHY

J.R. McMILLAN, PhD,[1] M. AKIYAMA, PhD,[1] F. ROUAN, PhD,[2] J.E. MELLERIO, MD,[3] E.B. LANE, PhD,[4] I.M. LEIGH, MD,[5] K. OWARIBE, PhD,[6] G. WICHE, PhD,[7] N. FUJII, MD,[8] J. UITTO, PhD,[2] R.A.J. EADY, DSc (Med),[3] and H. SHIMIZU, PhD[1]

[1] Department of Dermatology, Hokkaido University Graduate School of Medicine, Kita-ku, Sapporo 060-8638, Japan
[2] Department of Dermatology and Cutaneous Biology, Jefferson Medical College, Philadelphia, Pennsylvania USA
[3] St. John's Institute of Dermatology, King's College, St Thomas's Hospital, London, United Kingdom
[4] Department of Cell Structure, Department of Anatomy and Physiology, University of Dundee, United Kingdom
[5] Center for Cutaneous Research, St. Bartholomew's and the Royal London School of Medicine and Dentistry, Queen Mary Collage, London, United Kingdom
[6] Biosystems, Human Informatics, Nagoya University, Nagoya, Japan
[7] Department of Molecular Cell Biology, University of Vienna, Vienna, Austria
[8] Department of Neurology, National Omuta Hospital, Fukuoka, Japan

Accepted 27 July 2006

Genetic defects in the epidermal expression of plectin are known to form the basis of at least three disease subtypes: a rare, mild form of dominant epidermolysis bullosa simplex (EBS) with mottled pigmentation,[19,20] a severe recessive form of epidermolysis bullosa associated with pyloric atresia and severe loss of skin,[5,30,33] and a recessive form of EBS associated with muscular dystrophy (EBS-MD).[11,25,29,43,45,47] In EBS-MD, plectin defects are thought to affect plasma membrane–cytoskeletal interactions in skin and muscle causing epidermal blistering and late-onset muscle weakness.[11,25,29,45]

Plectin is a large, 450–500 kDa, cytoplasmic protein that acts as a link between various cytoskeletal systems and cell junctions.[50] In skin, plectin links the basal cell keratin intermediate filaments to the transmembrane collagen XVII[21] and the $\beta 4$ integrin subunit of the $\alpha 6\beta 4$ integrin located in the hemidesmosome.[22,23] In many tissues and cultured cells, plectin interacts with several cytoskeletal systems: actin microfilaments, intermediate filaments, or microtubules.[50] Plectin in different cells and tissue has the ability to interact with multiple binding partners including intermediate filaments (keratin, desmin, and vimentin), actin microfilaments, microtubules, and specialized molecules at specific junctions such

Abbreviations: BSA, bovine serum albumen; CT, computerized tomography; EBS-MD, recessive epidermolysis bullosa simplex associated with muscular dystrophy; GEL, gelatin; MRI, magnetic resonance imaging; NGS, normal goat serum; PBS, phosphate-buffered saline; PCR, polymerase chain reaction; TBS, Tris-buffered saline

Key words: plectin; intermediate filament; muscle; Z-line; epidermolysis bullosa

Correspondence to: J. R. McMillan; e-mail: jrm57@med.hokudai.ac.jp

Published online 11 September 2006 in Wiley InterScience (www.interscience.wiley.com). DOI 10.1002/mus.20655

as vinculin and β1 integrin in striated muscle costamere attachment sites[17,39,40,48] and Rack1.[32,42]

Multiple plectin isoforms are expressed in a tissue-specific manner in mammalian cells and tissues derived from a single gene, *PLEC1*.[7,10,36] In the mouse, plectin is expressed in at least 14 different isoforms, mostly resulting in different splice variants of the actin binding amino-terminal exon 2.[10] However, a form of plectin lacking all or part of the central rod domain (exons 31/32) has been proposed in the rat, similar to the system controlling dystrophin muscle expression.[7] More recently, distinct functions for different plectin isoforms have come to light after determining specific plectin isoform subcellular localization.[36]

Precise and complete isoform expression patterns in various human tissues including muscle have yet to be determined. However, intriguingly, muscle fiber type-specific expression patterns of plectin were reported in clinically normal and diseased human skeletal muscle[11,39] and at costamere membrane attachment sites.[18] Initial reports of control muscle staining with HD1-121 antibody suggested that HD1-121 stained Z-lines in type I muscle fibers, whereas other plectin antibodies (including the 10F6 and 5B3 antibodies) showed variable staining at the membrane.[11] EBS-MD muscle demonstrated a loss of membrane HD1-121 antibody staining with an unusual residual expression of sarcomere staining.[11] Further studies using control and diseased muscle have shown that plectin and desmin intermediate filaments closely encircle sarcomeres, as well as link to the plasma membrane.[4,11,16,38,40,41,43] More recently, in normal rat muscle plectin was suggested to associate with desmin at both vinculin- and dystrophin-containing plasma membrane junctions.[17]

In human skin plectin antibodies show two major epidermal staining patterns. First, a combined dermal–epidermal junction and suprabasal cytoplasmic pattern is seen with the majority of plectin antibodies (including 10F6, 5B3, 6C6,[52] and IFAP300, the hamster plectin homolog[44]). A second, dermal–epidermal junction restricted staining pattern is seen with the HD1-121 and plectin 7A8 antibodies.[25,45] Staining with all these antibodies is severely reduced or absent in EBS-MD patients' skin.[25,45] The binding sites of the majority of plectin antibodies have been identified as lying within the central rod domain including the HD1-121 antigen[15] and various rat plectin antibodies.[8,9,51,52] We now report the precise ultrastructural expression of plectin in normal human and EBS-MD muscle tissue using the most informative of the current battery of plectin antibodies. We have also examined the expression of important integral muscle components such as dystrophin, desmin, and α actinin in EBS-MD muscle. The aim of this study was to describe the plectin antibody expression patterns together with critical structural elements in striated muscle to determine the structure of plectin, its precise location, and likely function in striated muscle.

MATERIALS AND METHODS

Tissue Samples. Muscle and skin biopsy samples were obtained from three EBS-MD patients whose cases have been previously described.[34,45] All samples were collected after the patient's consent was obtained, with the relevant institutional approval for experiments involving human material in accordance with the principles of the Helsinki Declaration of 1975.

The clinical, histopathological, ultrastructural, and immunohistochemical details of skin findings (excluding mutation data), limited muscle histology, and immunohistochemistry from Case 1 were previously included in the report by Smith et al. (patient D3).[45] Case 1 was a man aged 33 years who had suffered from widespread friction-induced blistering of his skin since just after birth. He subsequently developed progressive muscle weakness before the age of 2 years and then became confined to a wheelchair. The family was of Maltese origin and the parents were related. Blistering was noted around the hands, feet, scalp, and face as he grew, and he developed hoarseness due to scarring of the anterior commissure of the larynx. He developed early onset and progressive muscular dystrophy before the age of 2 years and computerized tomography (CT) and magnetic resonance imaging (MRI) showed him to have cerebellar and cerebral atrophy. This patient was previously shown to have absent muscle plectin staining as highlighted by the antibody HD1-121.[6] Mutational analysis for this patient was performed here and is reported below.

Case 2 was a 10-year-old, fourth female child of Italian parents who were first cousins. Previously, mutations in the plectin gene (5905del2/5905del2) together with skin immunohistochemistry and ultrastructural findings in this patient were reported by Mellerio et al.[29] Case 2 also presented with widespread trauma-induced blistering on her fingers, hands, feet, and face shortly after birth. She experienced stridor associated with supraglottic scarring and stenosis from the first few weeks of life and underwent a tracheostomy at the age of 20 months because of recurrent episodes of respiratory embarrassment. The two elder siblings in the family were

unaffected. A third child had suffered from blistering and apneic episodes from birth and had died at age 4 years from respiratory obstruction.

The third case was a 45-year-old Japanese wheelchair-bound man, previously described by Pulkkinen et al.,[34,43] including the homozygous 5866delC/5866delC mutation, clinical details, and skin immunohistochemical and ultrastructural findings.

Electron microscopy of the skin biopsy from each patient indicated that blistering arose as a result of rupture of the basal epidermal cells at a level that was just above the keratinocyte plasma membrane[28,29,45] and these changes were associated with previously reported hemidesmosome structural abnormalities.[28] Specifically, EBS-MD Cases 1 and 2 showed poor hemidesmosome inner plaque assembly and keratin intermediate filament linkage to the hemidesmosome plaque.[36]

Control muscle samples (n = 5, in total) from the flexor digitorum (n = 1), gastrocnemius muscle (n = 2), and from paraspinal column (n = 2) were obtained from routine surgical procedures. Quadriceps muscle from patients with EBS-MD (n = 3) were biopsied under anesthesia for diagnostic purposes. The biopsy samples were divided and fixed for electron microscopy; they were snap-frozen in Tissue-Tek OCT compound (Miles Diagnostic, Elkhart, IN) using isopentane cooled by liquid nitrogen for cryostat sectioning or cryofixed for immunoelectron microscopy.

Mutation Detection. Genomic DNA was isolated from peripheral blood cells from the patient (in Case 1) and his immediate family members, and DNA from unrelated healthy individuals was used as a control. DNA was subject to polymerase chain reaction (PCR) followed by automated nucleotide sequencing of the PCR products. PCR amplification of exon 32 that contained the mutation was performed with the following primer pairs as previously described by Pulkkinen et al.[34]: Ex32 II L: 5′ GCTAATACGCATCACTATAGGAACAGACCACCATGTTCCG CGAGCTGGCCGAGG 3′; Ex32 R: 5′ TCACTTCTCCTTGAGCGCGATCT 3′.

The PCR products were subjected to automated sequencing using 12 overlapping primers covering the entire coding sequence of exon 32. The mutation was detected with Ex32 12/12 primers: sense, 5′ CTCAAGGCTGAGGCGGAACT 3′; antisense, 5′ TCACCCACCAAAGCGATCC 3′.

Light Microscopy and Immunohistochemistry. Immunohistochemical staining was performed with modifications previously described by McMillan et al.[26] Muscle cryostat sections (5 μm) were collected and dried on 3-aminopropyltriethoxysilane (APES)–coated slides (Sigma, Poole, UK). Sections were fixed in acetone (−20°C) for 10 min before being washed in 0.1 M Dulbecco's phosphate-buffered saline (PBS). Primary antibodies were diluted in 0.3% w/v bovine serum albumen (BSA) (ICN, Poole, UK) in PBS and were incubated for 30 min at 37°C in a humidified chamber. The primary antibodies used included the anti-HD1 antigen HD1-121,[15] dilution 1 in 50, which recognizes two distinct plectin rod domain epitopes that are likely closely related in the folded, native protein[31]; 5B3 and 10F6 (neat), both mouse monoclonal antibodies raised against the rod domain of rat plectin (from G. Wiche, Vienna, Austria[8]); and 4B4 raised against the β1 integrin (Beckman-Coulter, High Wycombe, UK), used at 1 in 200. Three antibodies recognizing three dystrophin antibodies were used: NCL-DYST1, NCL-DYST2, and NCL-DYST3 against the rod-, carboxyl-, amino-terminal domains (neat, 1 in 10, and 1 in 40, respectively; Novocastra, Newcastle upon Tyne, UK). Novocastra also supplied antibodies to β spectrin, (1 in 100), merosin (1 in 50), and β dystroglycan (1 in 50). Other antibodies and antiserum included were: desmin monoclonal D33 (Dako, High Wycombe, UK) 1 in 200; polyclonal desmin and vimentin (Sigma) used at 1 in 20, BM-75.2 against α actinin (Sigma) used at 1 in 200; and mouse anti-vinculin IgG (Sigma) used at 1 in 100. The slides were washed in PBS for 10 min, dried, and blocked with normal rabbit or goat serum (Dako) for 5 min, depending on the secondary antibody.

Immunoperoxidase. Consecutive 5-μm transverse frozen sections of normal and EBS-MD muscle were fixed in cold acetone, and endogenous biotin activity was blocked using 0.1% hydrogen peroxide. The immunohistochemical technique used streptavidin-biotin complexes coupled to horseradish peroxidase with diaminobenzidine visualization.[2] For primary antibody details, see the previous section. The secondary antibody was rabbit antimouse peroxidase conjugated and was diluted 1 in 500 (Dako) or biotin conjugated goat antimouse (1 in 500) followed by peroxidase conjugated streptavidin (diluted 1 in 1,000). Routine enzyme histochemistry fiber typing was performed by staining with NADPH and ATPase preparations at pH 9.4, 4.6, and 4.3. All experiments included appropriate positive and negative controls and were performed in duplicate.

Immunofluorescence. The secondary antibody dilution was 1 in 500 in 0.3% BSA in PBS. The secondary

Table 1. Details of the patients having epidermolysis bullosa simplex with muscular dystrophy.

	Case 1	Case 2	Case 3
Patient age, origin, muscle biopsy site, parental relationship	Male, 33 y, Maltese origin, quadriceps biopsy, consanguineous	Female, 10 y, Italian origin, quadriceps biopsy, consanguineous	Male, 45 y, Japanese origin, thigh muscle biopsy, consanguineous
PLEC1 mutation/site	R2465X/R2465X* Exon 32	5905del2/5905del2 Exon 31	5866delC/5866delC Exon 31
References			
Mutation report	R2465X/R2465X*	Mellerio et al.[29]	Pulkkinen et al.[34]
Clinical report	Smith et al.[45]	Smith et al.[45]	Pulkkinen et al.[34]

* *Novel mutation detailed in this report.*

antibodies used were rabbit antimouse FITC (Dako) or goat antimouse FITC (Dako) and donkey antirabbit Texas red (Amersham, Amersham, UK) and goat antimouse Texas red (Amersham). The muscle and skin sections were incubated for 30 min at 37°C in a dark chamber and then washed in PBS. Sections were dried in the dark and mounted in a 10% PBS/glycerol anti-fade mountant. All experiments included appropriate positive and negative controls and were performed in duplicate.

Transmission Electron Microscopy. Control muscle specimens (gastrocnemius and flexor digitorum, n = 2) and EBS-MD muscle (n = 3) were cut, attached to an immovable cork surface, fixed in half-strength Karnovsky's fixative containing 2% formaldehyde and 2.5% glutaraldehyde,[18] and routinely processed as described by McMillan and Eady[27] for electron microscopy. Briefly, samples were washed in 0.067 M cacodylate buffer; osmium postfixation was in 1.3% osmium for 2 h at room temperature. Specimens were stained en bloc in 5% uranyl acetate in 50% ethanol (1 h), dehydrated in a graded ethanol series (15 min each), and embedded in TAAB 812 or Araldite resin with hard hardener (TAAB, Aldermaston, UK) via propylene oxide (two washes). Semithin and ultrathin sections were cut on a Reichert OMU-4 ultramicrotome (Leica, Milton Keynes, UK). Semithin sections (0.5 μm thick) were stained with azure II and methylene blue.[37] Ultrathin sections (60–90 nm) were collected on copper grids, stained in 50% alcoholic uranyl acetate and lead citrate, and examined in either a JOEL 100CX or Hitachi H7100 electron microscope with an accelerating voltage of 75 kV.

Immunoelectron Microscopy. Muscle cryofixation and cryosubstitution was carried out as previously described.[26] Briefly, control muscle samples (calf leg muscle and control flexor digitorum muscle, n = 2) were cut, cryoprotected, and plunged into liquid propane cooled by liquid nitrogen in a Leica KF 80 freeze plunging machine. The EBS-MD muscle sample was taken from the thigh leg muscle (Table 1).

Samples were then placed in methanol at −80°C for 3 days in either an AFS or a CS AUTO freeze substitution machine (Reichert, Depew, New York). The samples were embedded in Lowicryl K11M resin/methanol mixtures at −60°C for 4 days while the percentage of Lowicryl K11M resin mixture was increased. The samples were embedded in K11M resin while being polymerized under an ultraviolet light in a dry nitrogen atmosphere. The edges of the blocks were sectioned to check orientation and ultrastructure. Ultrathin sections of 90-nm thickness were collected on pioloform-coated nickel grids and stored for immunolabeling.

Labeling was carried out by floating the nickel grids on drops of buffer in a clean, humid chamber. The grids were incubated in PBS containing 5% normal goat serum (NGS), 1% gelatin (GEL), and 1% bovine serum albumin (BSA) for 30 min. Primary antibodies were diluted in 1% NGS, 1% GEL, 1% BSA in PBS for 1 h followed by four PBS washes. All gold-conjugated antibodies were diluted in 0.2 M Tris-buffered saline (TBS), pH 8.2, with 1% NGS, 1% GEL, and 1% BSA. The secondary antibodies were 5- or 15-nm gold-conjugated goat antimouse and 5- or 15-nm gold-conjugated goat antirabbit (Biocell, Cardiff, UK). The grids were washed twice in TBS and distilled water and stained with 2.5% uranyl acetate in 50% ethanol for 15 min and observed. For each control or EBS-MD sample a total of 7–10 blocks were examined.

RESULTS

Mutation Detection. DNA isolated from peripheral blood cells of the patient (Case 1) with EBS-MD (Fig. 1A) and his parents was subjected to mutation detection analysis. Proband DNA underwent direct nucleotide sequencing for the entire intron–exon borders of the plectin gene. Direct nucleotide sequencing of exon 32 PCR products

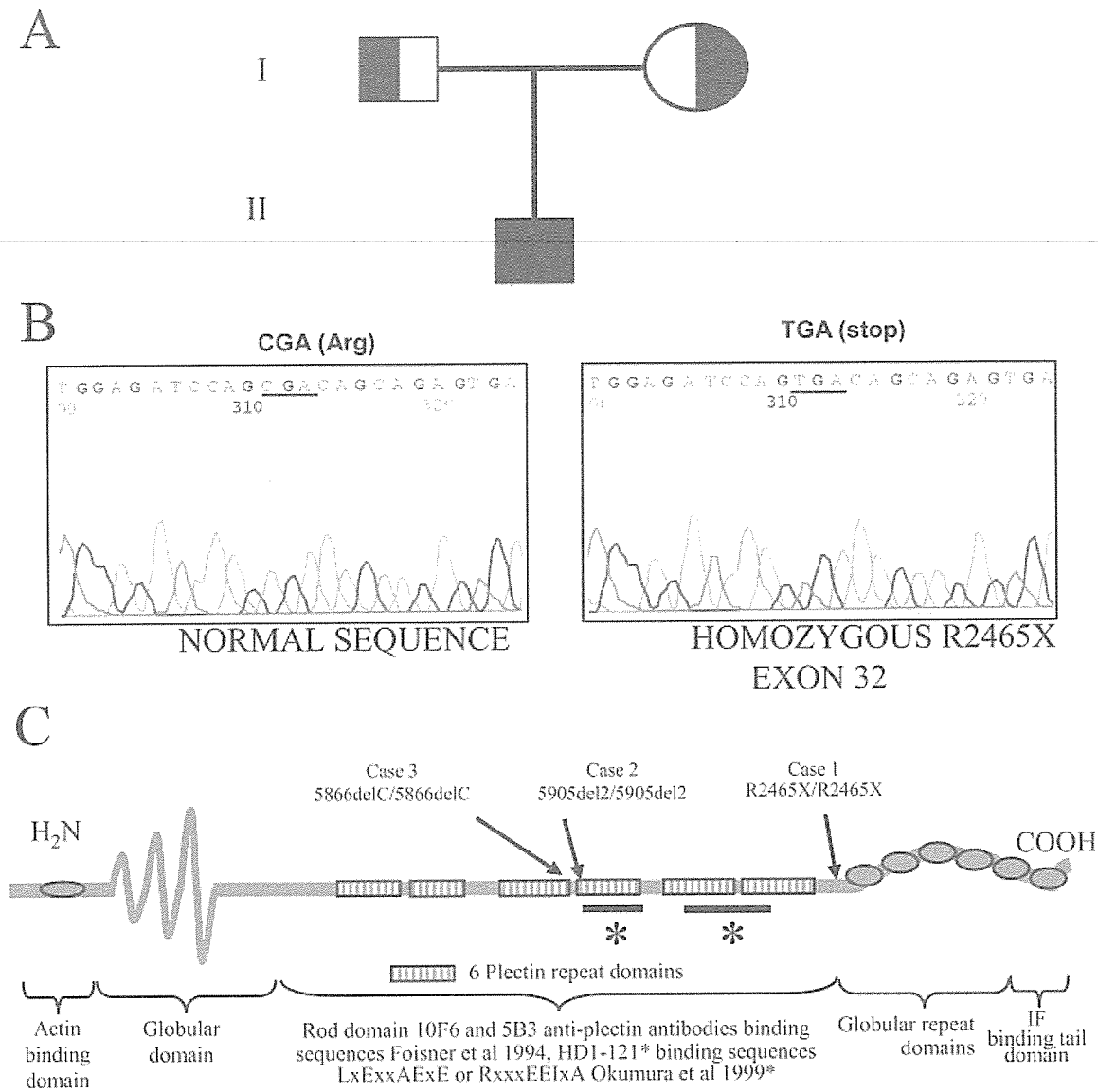

FIGURE 1. Mutation detection by automated nucleotide sequencing in a Maltese family with epidermolysis bullosa simplex and muscular dystrophy (EBS-MD). **(A)** Pedigree of the family from Case 1 with the proband suffering from EBS-MD. **(B)** Direct nucleotide sequencing of Ex32 PCR products revealed that the proband is homozygous for a C–T transition in nucleotide position 7444. This nucleotide substitution results in the change of an arginine residue (CAG) to a stop codon (TAG), and this mutation was designated R2465X. Predictions suggest that this mutation should lead to nonsense-mediated mRNA decay and a severe reduction or absence of plectin expression. **(C)** Summary of mutations in the three EBS-MD cases whose muscle findings are included in this report. Below, a schematic highlighting plectin domains and the binding sites of the three plectin antibodies (10F6/5B3/HD1-121) used in this study. The precise binding site in the rod domain of 5B3 and 10F6 antibodies is unknown (G. Wiche, personal communication).

revealed that the proband was homozygous for a C–T transition in nucleotide position 7444 when compared to unrelated, healthy individuals (n = 50). This nucleotide substitution resulted in a change of an arginine residue (CAG) to a stop codon (TAG), and this mutation was designated R2465X. We predict that this mutation will lead to nonsense-mediated mRNA decay and to a severe reduction or absence of plectin expression. The site of this mutation is at the very terminal, car-

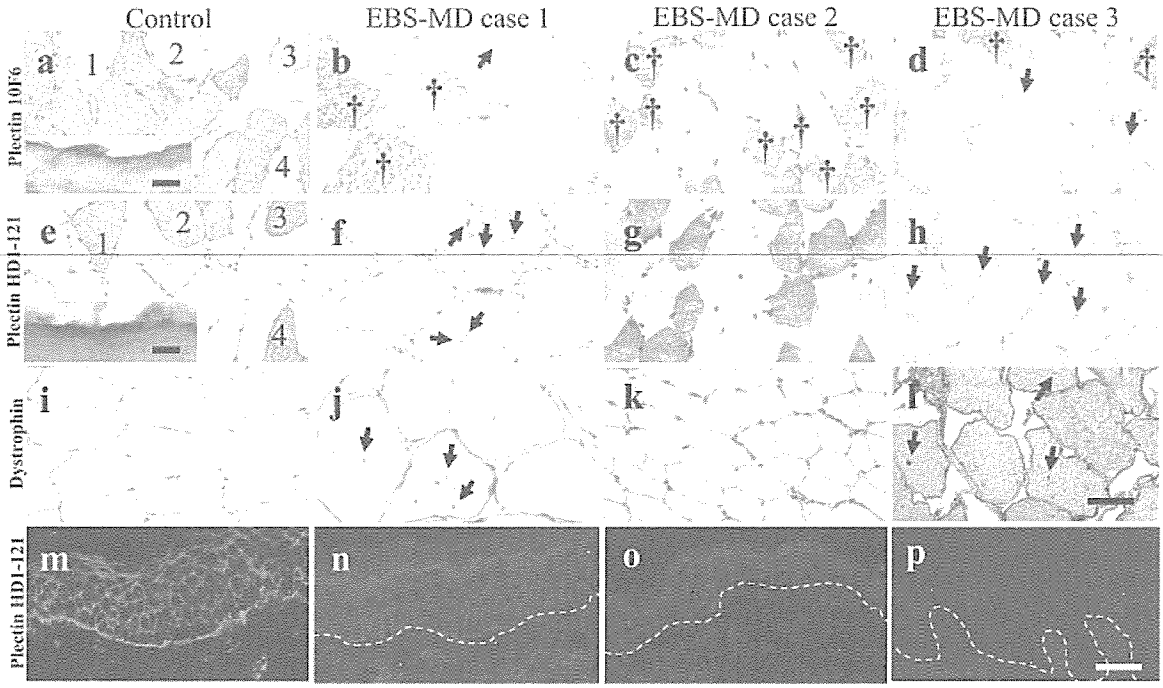

FIGURE 2. Loss of plectin expression at the periphery of all EBS-MD muscle fibers compared to control muscle myocytes. Plectin stained the membrane periphery of all control muscle fibers using all antibodies but only the center of selected fibers with the 10F6 antibody (**a** and inset) and the HD1-121 antibody (**e** and inset). However, plectin antibodies 10F6 **(b–d)** and HD1 **(f–h)** showed no staining at the cell periphery in all three EBS-MD patient muscle samples. In control type II muscle fibers, plectin (10F6) is expressed at the sarcolemma and within the cytoplasm but is restricted to the periphery of type I fibers. Conversely, plectin-HD1 is expressed at the periphery of all (type I and II) control muscle fibers but is restricted to the central cytoplasm of type I fibers. In EBS-MD muscle, plectin **(b–d)** and HD1 **(f–h)** expression is absent at the periphery of all muscle fibers. However, plectin expression is retained within the center of type II fibers in all EBS-MD cases together with multiple internalized nuclei (arrows). In comparison, HD1 was expressed in the center of type II fibers in only one case of EBS-MD muscle (Case 2, **g**). Thus, there is a profound reduction or loss of both plectin 10F6 and HD1-121 staining at the plasma membrane in EBS-MD tissue. In the youngest EBS-MD case **(g)** HD1 shows some cytoplasmic staining, but no staining occurs in the other cases **(f,h).** Control muscle **(i)** and EBS-MD muscle **(j–l)**, showed normal peripheral dystrophin staining. Control skin showed linear staining **(m)** for plectin HD1-121, but in EBS-MD patients skin this staining was absent **(n–p)**. Inset **(a,e)** scale bar, 20 μm. Scale bar, 100 μm.

boxyl end of the rod domain that is encoded for by exon 32. Three different EBS-MD mutations in our patients' R2465X/R2465X (reported here for the first time, to our knowledge), 5866delC/5866delC, and 5905del2/5905del2 were located within the same plectin rod domain (Fig. 1C) and were all predicted to result in a severe reduction or ablation of full-length plectin expression in skin and skeletal muscle through nonsense-mediated mRNA decay. Any exon-specific plectin splicing involving the rod domain (as previously suggested[7,10,36]) could theoretically lead to some persistent plectin isoforms expression within certain organs and tissues.

Light Microscopy and Immunohistochemistry. Light microscope findings in Case 1 were previously reported briefly by us.[45] The appearances of the muscle biopsies particularly from the two oldest cases (Cases 1 and 3) were that of a chronic myopathy (Fig. 2b,d,f,h,j,l) sharing many of the histological features previously described.[3,45] There was wide variation in striated muscle-fiber size, the largest being hypertrophied, measuring more than 150–200 μm. There were both individual and grouped atrophic fibers. There were also increases in the amount of endomysial and perimysial connective tissue. Pyknotic nuclear clumps were present, and several fibers displayed multiple, internal nuclei (Fig. 2), as previously described.[45] There was evidence of continuing muscle-fiber necrosis: scattered fibers undergoing phagocytosis were observed and there were several hyaline (segmentally necrotic) myocytes. A few regenerating fibers were also observed. Case 3 also showed the formation of very small vacuoles at

the edge of occasional fibers that were not observed in Cases 1 or 2. Case 2, the youngest case included in this study, showed a very mild variation in myocyte fiber size but was otherwise unremarkable.

Immunoperoxidase. Plectin was localized in control muscle (using both 10F6 and 5B3 antibodies) to the membranes of both type I and type II fibers (Fig. 2a). Plectin was also expressed throughout the center of type II muscle fibers (see Fig. 2a), as defined by ATPase staining at pH 9.4, 4.6, and 4.3 (data not shown). This HD1-121 fiber type–specific finding was in agreement with the report of Gache et al.[11] In control muscle the majority (60%) of all muscle fibers exhibited staining for plectin within the center of the fibers. In EBS-MD Cases 1 and 3, plectin expression (using the same two antibodies) was completely absent from the plasma membrane and expressed in a speckled pattern within the center of 50%–60% of type II muscle fibers. Case 2 showed a similar loss of plectin immunoreactivity at the plasma membrane but a normal persistence of plectin expression within type II fibers (Fig. 2c).

Conversely, in control muscle the HD1 plectin antigen (recognized by the HD1-121 antibody) was expressed at the plasma membrane (Fig. 2e) of both type I and II muscle fibers. This showed similar staining patterns to previously reported plectin in muscle.[11] However, HD1 showed restricted expression within the center of type I fibers (see fibers with asterisks in Fig. 2e). HD1 antigen expression in the center of type II muscle cells was complementary (i.e., the exact reverse) of the plectin (10F5 and 5B3) staining observed in type I muscle fibers. Less than half of all control muscle fibers examined (between 30%–40%) exhibited this central HD1-121 staining pattern.

In EBS-MD muscle there was a loss of plasma membrane plectin and HD1 expression (in all plectin-deficient cases, Fig. 2f–h). In the majority of EBS-MD muscle (Cases 1 and 3, Figs. 2f,h) there was no HD1 expression within any of the muscle fibers except in Case 2 (Fig. 2g), where there was residual staining within the center of type I fibers. In control (Fig. 2i) and EBS-MD muscle (Fig. 2j–l), dystrophin stained the periphery of both types I and II muscle fibers. In all EBS-MD cases there was also a normal staining pattern for the integrin $\beta 1$ subunit, β spectrin, merosin, β dystroglycan, and vinculin similar to control muscle. Vimentin was expressed in selected muscle-fibers from EBS-MD cases 1 and 3 but not in control muscle.

Longitudinal muscle sections of α actinin and desmin staining (both Z-line–associated proteins) produced a regular banded pattern of staining in control muscle, but in EBS-MD muscle from Cases 1 and 3 this pattern was weak or severely, focally disrupted. An abnormal increase or clumping of α actinin and desmin staining was observed at the periphery of EBS-MD fibers in Case 1. Thus, the normal, striated pattern of the intermediate filament protein desmin (linking adjacent Z-lines and Z-lines to the plasma membrane) and α actinin, a structural protein and constituent of the Z-line, were disrupted in EBS-MD compared to control muscle.

Immunofluorescence. In control skin, bright, linear fluorescence was noted along the dermal–epidermal junction and within the cytoplasm of suprabasal keratinocytes (Fig. 2m) for plectin HD1-121, but in EBS-MD patients' skin this staining was completely absent (Fig. 2n–p). All other plectin antibodies including HD1-121, 10F6, 5B3, and 7A8[9] showed similar or identical skin staining patterns. This expression of plectin in EBS-MD skin was reported previously.[25,34,45]

Transmission Electron Microscopy. The most striking ultrastructural change in EBS-MD muscle was the increased space between the plasma membrane and the muscle sarcomere, seen in EBS-MD muscle (Fig. 3b,d) but not in controls (Fig. 3a). Case 1 (Fig. 3b) contained enlarged spaces between the folded plasma membrane and contractile units. This was a consistent finding in all five biopsy specimens. In addition, there was extensive reduplication of the basement membrane (Fig. 3b) caused by successive fiber necrosis and regeneration events. Small "focal densities" on the plasma membrane, associated with cytoskeletal filaments, were seen at regular intervals on the cytoplasmic surface of the plasma membrane in both control and EBS-MD muscle fibers (Fig. 3a, vs. 3b,d, respectively). The structure of these densities was unaffected by the muscle fiber pathology. Ultrastructural investigation of EBS-MD muscle from the youngest patient (Case 2, four samples) showed relatively mild myocyte disorganization and only very limited enlargement of the space between the membrane and the plasma membrane.

Comparison of control muscle (Fig. 3a) and EBS-MD muscle (Case 1, Fig. 3b,c; Case 3, Fig. 3d,e) revealed a focal loss of normal sarcomere organization in selected muscle fibers that appeared to resemble a fiber type–specific grouped pattern. However, the severe pathological changes in the EBS-MD muscle tissue made accurate ultrastructural fiber typing difficult (Fig. 3b–f). A further striking ultrastructural change in EBS-MD Cases 1 and 3 were the areas

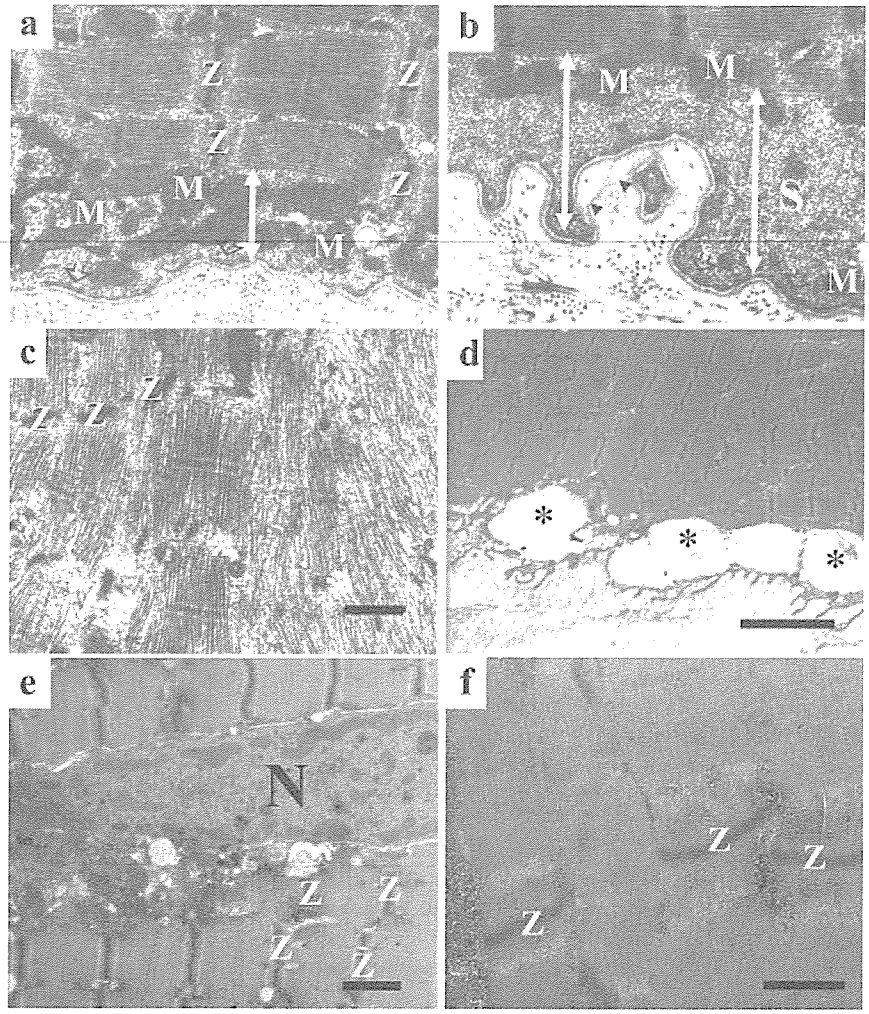

FIGURE 3. Muscle of patients with EBS-MD shows a severe loss of normal sarcomere organization and Z-line-plasma membrane anchorage. Transmission electron microscopy of muscle from normal control **(a)** and EBS-MD patients' muscle **(b–e)**. Compared to control muscle tissue **(a)**, EBS-MD muscle **(b)** shows a variably enlarged space (S, white arrow) between the plasma membrane and the muscle contractile units (sarcomeres). In both normal muscle **(a)** and EBS-MD Case 1 **(b)**, small electron densities were seen on the cytoplasmic surface of the plasma membrane (open arrows) **(a,b,d)**. Mitochondrial distributions within the normal parameter limits (M) were seen in the spaces beneath the plasma membrane both in normal and EBS-MD muscle. EBS-MD Case 1 also showed extensive basement membrane reduplication, suggesting that repetative fiber atrophy and regeneration had taken place **(b**, arrowheads). In a subset of myocytes there was focal loss of normal sarcomere organization **(c)** including the presence of small or disorganized Z-lines (Z) or a loss of Z-lines (asterisk, in **c**). In muscle from Case 3 **(d–f)**, similar sarcomere changes were present but in addition there were large vacuolated areas adjacent to the plasma membrane (asterisks in **d**). Within the center of muscle fibers in Case 3 there was a mild disorganized misalignment of sarcomeres and focal variability in Z-line size (Z in **e,f**). Abnormal, centrally located myocyte nuclei (N) were also observed **(e)**. Biopsies from Cases 1 and 3 both showed enlarged spaces between the myofibrillar apparatus and the myocyte plasma membrane and contained thin filaments that were possibly lost from the edge of the sarcomeres **(b,d)**. Scale bars: 1 μm **(a–c,e)**; 5 μm **(d)**; 0.5 μm **(f)**.

of focal myofibrillar disorganization. The loss of normal sarcomere organization was chiefly characterized by focal loss of or variation in normal Z-line size and alignment (Fig. 3). The width of the sarcomere unit and length of Z-lines were often thinner and smaller than controls (Fig. 3). This variation in Z-line size was beyond the normal variation observed in either type I or II fibers.[12,13] Where sarcomeres remained intact, they were incomplete or misaligned with their neighboring sarcomeres (Fig. 3b–f).

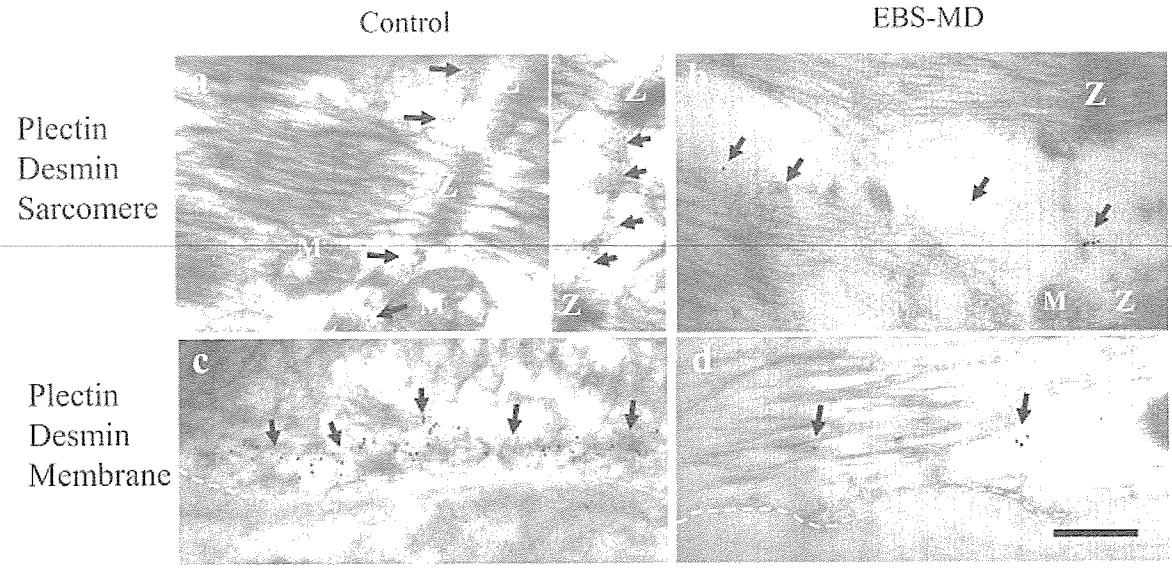

FIGURE 4. Plectin is coexpressed in control muscle with the intermediate filament protein desmin between adjacent Z-lines and between peripheral Z-lines and the plasma membrane, but this pattern is disrupted in plectin-deficient muscle. Double-labeling using immunogold electron microscopy in control muscle shows numerous plectin (5B3, small 5-nm gold particles) and desmin (larger 15-nm particles) labeling (arrows in **a**, and inset) adjacent to Z-lines (Z) but sparse labeling between Z-lines in EBS-MD muscle (arrows in **b**). In control muscle **(a)**, mitochondria (M) were regularly seen close to or adjacent to Z-lines (Z). In EBS-MD muscle (Case 3) Z-line plectin and desmin labeling **(b)** was severely reduced and disrupted compared to controls (see inset **b**). Furthermore, in control muscle significantly greater densities of plectin and desmin labeling were observed adjacent to the plasma membrane (arrows in **c**). In contrast, the periphery and plasma membrane of EBS-MD muscle showed significantly reduced plectin and desmin staining (arrows in **d**). Scale bar, 100 nm.

There was little uniformity between sarcomeres; thick and thin filaments could regularly be seen running at a tangent to the plasma membrane. The thick and thin filaments were observed at the edge of the sarcomere and often became extruded into the spaces between the sarcomeres (Fig. 3c). Z-line smearing was apparent in focal areas of sarcomere disorganization (Fig. 3c) but was not associated with any abnormal storage material within the myocyte. The loss of myofibrils was replaced by amorphous material, glycogen and swollen sarcoplasmic reticulum cisternae. The number and position of mitochondria at the cell periphery adjacent to the sarcomeres was within normal limits, occasionally showing a mild disruption in distribution in Cases 1 and 3.

Immunoelectron Microscopy. Double-labeling immunogold electron microscopy of control muscle fibers colocalized plectin (5B3) and desmin to between Z-lines (Fig. 4a,b). The muscle intermediate filament protein desmin showed a similar colocalization with HD1 in all fiber types. Mitochondria could be seen close to the Z-lines in control muscle (Fig. 4a). In EBS-MD muscle there was a severe loss or reduction and disruption in both plectin and desmin staining (Fig. 4b) compared to control muscle (Fig. 4a vs. 4b). Plectin and desmin colocalized to beneath the cytoplasmic face of small electron densities underlying the sarcolemma in control muscle (Fig. 4c), but in EBS-MD muscle there was a severe loss or reduction in this staining (Fig. 4d).

EBS-MD muscle also showed normal expression of all dystrophin antibody staining (including N- and C-terminal epitopes) in a regular fashion over small, discrete densities along the plasma membrane in a similar fashion to that observed in control muscle. Immunogold particle (5 nm) distribution along the plasma membrane demonstrated similar expression of the integrin $\beta 1$ subunit in control and EBS-MD muscle.

DISCUSSION

There are several major findings in this report. First, plectin (using all the plectin antibodies in this study) is expressed adjacent to the myocyte membrane in control type I and type II muscle fibers. However, multiple plectin antibodies show distinct fiber type–specific expression patterns within the center of normal type II muscle fibers. Conversely, staining for plectin with the HD1-121 antibody was restricted within the center of control type I muscle fibers.

From our data, we suggest that plectin or a closely related molecule is expressed in multiple fiber-specific isoforms comprising different rod domain sequences.[7,10] The significance of different plectin isoforms in at least these two subcellular locations, in the center of the muscle fiber between Z-lines and adjacent to the plasma membrane, is likely to be related to multiple crosslinking functions. In the center of the muscle fiber, plectin crosslinks the intermediate filaments desmin and vimentin (in regenerating fibers) running between Z-lines, and therefore might indirectly link Z-lines via interactions with components such as α actinin (a Z-line component).

At the muscle-fiber periphery, possible plectin-binding partners include desmin intermediate filaments, but also actin, vinculin, and α actinin at costamere β1 integrin-containing junctions.[38,40] The previously reported close association of plectin with costameres does not preclude it from association with dystrophin complex components; however, our data show no alterations in dystrophin proteins in EBS-MD muscle. In EBS-MD muscle there was a severe disruption in normal plectin, α actinin (a Z-line component), and desmin organization, suggesting that plectin is critical for normal sarcomere arrangement. Vimentin is an intermediate filament protein expressed in regenerating muscle, and was frequently observed in EBS-MD cases 1 and 3. Myocyte damage in plectin-deficient muscle may result from an uneven transfer of contractile energy between Z-lines and from Z-line to the myocyte costamere–plasma membrane via the desmin cytoskeleton. However, plectin may also play an additional role in supporting the normal vimentin-cytoskeleton during muscle-fiber regeneration. Plectin therefore might play multiple roles in EBS-MD pathogenesis.

In addition, plectin is thought to be responsible for maintaining the shape and mechanical stability of the myocyte between the Z-line and the myocyte plasma membrane.[14,24] Ultrastructurally, plectin- and desmin-deficient muscle share many similar features.[14,24] However, the loss of desmin was reported to cause more severe Z-line and sarcomere disruption than was seen in our plectin-deficient samples.[16]

A further significant finding was the loss of plectin staining from all EBS-MD patient tissue at the periphery of muscle fibers. Previously, plectin and HD1-121 had been reported present just within the myocyte membrane, and reduced or absent staining was reported in EBS-MD.[11] The colocalization of plectin and desmin intermediate filaments parallel to Z-lines suggests a role in the attachment and organizing of these structures. In addition, our studies colocalized plectin and desmin to the region immediately beneath the myocyte plasma membrane, which underlines the importance of anchorage between the cytoskeleton and the plasma membrane, analogous to hemidesmosomes in epithelia. In EBS-MD muscle the loss of membrane–intermediate filament connections via plectin caused increases in subsarcolemmal space and frequent juxtamembrane vacuolization, again highlighting the importance of cytoskeletal–plasma membrane anchorage in normal muscle.

A recently proposed role for desmin–mitochondrial interactions was not supported by a significant displacement of mitochondria in our EBS-MD muscle samples.[1,6,35] Proper uniform subcellular localization of mitochondria within the muscle fiber is essential for efficient energy transfer to the sarcomere, and hence correct muscle function, but may be a relatively minor contributing factor to the late-onset muscle weakness seen in EBS-MD.[35,36,46,49] However, we cannot rule out the possibility that a subtle redistribution of mitochondria may result in some loss of contractile capability in EBS-MD muscle. Further specific mitochondria staining and oxidative phosphorylation studies are required to investigate this.

From our data, it seems that plectin is vital in linking multiple proteins at different sites within muscle fibers to the cytoskeleton. Plectin deficiency in muscle has serious deleterious effects on the transmission of contractile forces from the adjacent sarcomeres via the desmin cytoskeleton to the plasma membrane and leads to the progressive pathological changes seen in this disorder. Elucidation of the full range of molecular interactions between plectin isoforms and the myocyte cytoskeleton will pave the way for a better understanding of the pathogenesis of EBS-MD and other muscular dystrophies.

Presented at the European Society for Dermatological Research and the Society for Investigative Dermatology, April 2004. We thank Dr. Jennian Geddes, Ms. Megumi Sato, and Dr. Osamu Shirado for significant contributions to this work. We thank Prof. D. Landon (Institute of Neurology, London) for comments and advice on this study. Supported by the Welcome Trust (to E.B.L., I.M.L., R.A.J.E.), the Muirhead Trust (to R.A.J.E.) and the Special Trustees of St. Thomas' Hospital (to R.A.J.E.), by a grant-in-aid for Scientific Research A (13357008, to H.S.) and a grant from the Japanese Health Science Foundation (to J.R.M., H.S.) and by a grant-in-aid from the Health and Labor Sciences Research Grant for research into specific diseases H17-Saisei-12 (to J.R.M.).

REFERENCES

1. Appaix F, Kuznetsov AV, Usson Y, Kay L, Andrienko T, Olivares J, et al. Possible role of cytoskeleton in intracellular arrangement and regulation of mitochondria. Exp Physiol 2003;88:175–190.

2. Bancroft JD, Stevens A. Theory and practice of histological techniques, Vol. 1. London: Churchill Livingstone; 1996. p 343–364.
3. Banwell BL, Russel J, Fukudome T, Shen XM, Stilling G, Engel AG. Myopathy, myasthenic syndrome, and epidermolysis bullosa simplex due to plectin deficiency. J Neuropathol Exp Neurol 1999;58:832–846.
4. Carlsson L, Li ZL, Paulin D, Price MG, Breckler J, Robson RM, et al. Differences in the distribution of synemin, paranemin, and plectin in skeletal muscles of wild-type and desmin knockout mice. Histochem Cell Biol 2000;114:39–47.
5. Charlesworth A, Gagnoux-Palacios L, Bonduelle M, Ortonne J-P, De Raeve L, Meneguzzi G. Identification of a lethal form of epidermolysis bullosa simplex associated with a homozygous genetic mutation in plectin. J Invest Dermatol 2004;121: 1344–1348.
6. Costa ML, Escaleira R, Cataldo A, Oliveira F, Mermelstein CS. Desmin: molecular interactions and putative functions of the muscle intermediate filament protein. Braz J Med Biol Res 2004;37:1819–1830.
7. Elliott CE, Becker B, Oehler S, Castanon MJ, Hauptmann R, Wiche G. Plectin transcript diversity: identification and tissue distribution of variants with distinct first coding exons and rodless isoforms. Genomics 1997;42:115–125.
8. Foisner R, Feldman B, Sander L, Seifert G, Artlieb U, Wiche G. A panel of monoclonal antibodies to rat plectin: distinction by epitope mapping and immunoreactivity with different tissues and cell lines. Acta Histochem 1994;96:421–438.
9. Foisner R, Feldman B, Sander L, Wiche G. Monoclonal antibody mapping of structural and functional plectin epitopes. J Cell Biol 1991;112:397–405.
10. Fuchs P, Zorer M, Rezniczek GA, Spazierer D, Oehler S, Castanon MJ, et al. Unusual 5' transcript complexity of plectin isoforms: novel tissue-specific exons modulate actin binding activity. Hum Mol Genet 1999;8:2461–2472.
11. Gache Y, Chavanas S, Lacour JP, Wiche G, Owaribe K, Meneguzzi G, et al. Defective expression of plectin/hd1 in epidermolysis bullosa simplex with muscular dystrophy. J Clin Invest 1996;97:2289–2298.
12. Gauthier GF. Ultrastructural identification of muscle fiber types by immunocytochemistry. J Cell Biol 1979;82:391–400.
13. Gauthier GF, Lowey S. Distribution of myosin isoenzymes among skeletal muscle fiber types. J Cell Biol 1979;81:10–25.
14. Goebel HH. Desmin-related neuromuscular disorders. Muscle Nerve 1995;18:1306–1320.
15. Hieda Y, Nishizawa Y, Uematsu J, Owaribe K. Identification of a new hemidesmosomal protein, hd1: a major, high molecular mass component of isolated hemidesmosomes. J Cell Biol 1992;116:1497–1506.
16. Hijikata T, Murakami T, Imamura M, Fujimaki N, Ishikawa H. Plectin is a linker of intermediate filaments to z-discs in skeletal muscle fibers. J Cell Sci 1999;112:867–876.
17. Hijikata T, Murakami T, Ishikawa H, Yorifuji H. Plectin tethers desmin intermediate filaments onto subsarcolemmal dense plaques containing dystrophin and vinculin. Histochem Cell Biol 2003;119:109–123.
18. Karnovsky MJA. Formaldehyde-glutaraldehyde fixative of high osmolarity for use in electron microscopy. J Cell Biol 1965;27:137–138a.
19. Koss-Harnes D, Hoyheim B, Anton-Lamprecht I, Gjesti A, Jorgensen RS, Jahnsen FL, et al. A site-specific plectin mutation causes dominant epidermolysis bullosa simplex ogna: two identical de novo mutations. J Invest Dermatol 2002;118:87–93.
20. Koss-Harnes D, Jahnsen FL, Wiche G, Soyland E, Brandtzaeg P, Gedde-Dahl T, Jr. Plectin abnormality in epidermolysis bullosa simplex ogna: non-responsiveness of basal keratinocytes to some anti-rat plectin antibodies. Exp Dermatol 1997; 6:41–48.
21. Koster J, Geerts D, Favre B, Borradori L, Sonnenberg A. Analysis of the interactions between BP180, BP230, plectin and the integrin alpha6beta4 important for hemidesmosome assembly. J Cell Sci 2003;116:387–399.
22. Koster J, van Wilpe S, Kuikman I, Litjens SH, Sonnenberg A. Role of binding of plectin to the integrin beta4 subunit in the assembly of hemidesmosomes. Mol Biol Cell 2004;15:1211–1223.
23. Litjens SH, Wilhelmsen K, de Pereda JM, Perrakis A, Sonnenberg A. Modeling and experimental validation of the binary complex of the plectin actin binding domain and the first pair of fnIII domains of the β4 integrin. J Biol Chem 2005;280: 22270–22277.
24. Liu CG, Maercker C, Castanon MJ, Hauptmann R, Wiche G. Human plectin: organization of the gene, sequence analysis, and chromosome localization (8q24). Proc Natl Acad Sci U S A 1996;93:4278–4283.
25. McLean WHI, Pulkkinen L, Smith FJ, Rugg EL, Lane EB, Bullrich F, et al. Loss of plectin causes epidermolysis bullosa with muscular dystrophy: cDNA cloning and genomic organization. Genes Dev 1996;10:1724–1735.
26. McMillan JR, Akiyama M, Nakamura H, Shimizu H. Colocalization of multiple laminin isoforms predominantly beneath hemidesmosomes in the upper lamina densa of the epidermal basement membrane. J Histochem Cytochem 2006;54:109–111.
27. McMillan JR, Eady RA. Hemidesmosome ontogeny in digit skin of the human fetus. Arch Dermatol Res 1996;288:91–97.
28. McMillan JR, McGrath JA, Tidman MJ, Eady RA. Hemidesmosomes show abnormal association with the keratin filament network in junctional forms of epidermolysis bullosa. J Invest Dermatol 1998;110:132–137.
29. Mellerio JE, Smith FJ, McMillan JR, McLean WHI, McGrath JA, Morrison GA, et al. Recessive epidermolysis bullosa simplex associated with plectin mutations: infantile respiratory complications in two unrelated cases. Br J Dermatol 1997;137: 898–906.
30. Nakamura H, Sawamura D, Goto M, McMillan JR, Park S, Kono S, et al. Epidermolysis bullosa simplex associated with pyloric atresia is a novel clinical subtype caused by mutations in the plectin gene (plec1). J Mol Diagn 2005;7:28–35.
31. Okumura M, Uematsu J, Hirako Y, Nishizawa Y, Shimizu H, Kido N, et al. Identification of the hemidesmosomal 500 kda protein (hd1) as plectin. J Biochem (Tokyo) 1999;126:1144–1150.
32. Osmanagic-Myers S, Wiche G. Plectin-rack1 (receptor for activated c kinase 1) scaffolding: a novel mechanism to regulate protein kinase c activity. J Biol Chem 2004;279:18701–18710.
33. Pfendner E, Uitto J. Plectin gene mutations can cause epidermolysis bullosa with pyloric atresia. J Invest Dermatol 2005; 124:111–115.
34. Pulkkinen L, Smith FJ, Shimizu H, Murata S, Yaoita H, Hachisuka H, et al. Homozygous deletion mutations in the plectin gene (plec1) in patients with epidermolysis bullosa simplex associated with late-onset muscular dystrophy. Hum Mol Genet 1996;5:1539–1546.
35. Reimann J, Kunz WS, Vielhaber S, Kappes-Horn K, Schroder R. Mitochondrial dysfunction in myofibrillar myopathy. Neuropathol Appl Neurobiol 2003;29:45–51.
36. Rezniczek GA, Abrahamsberg C, Fuchs P, Spazierer D, Wiche G. Plectin 5'-transcript diversity: short alternative sequences determine stability of gene products, initiation of translation and subcellular localization of isoforms. Hum Mol Genet 2003;12:3181–3194.
37. Richardson KC, Jarret L, Finke EH. Embedding in epoxy resins for ultrathin sectioning in electron microscopy. Stain Technol 1960;35:313–323.
38. Schroder R, Kunz WS, Rouan F, Pfendner E, Tolksdorf K, Kappes-Horn K, et al. Disorganization of the desmin cytoskeleton and mitochondrial dysfunction in plectin-related epidermolysis bullosa simplex with muscular dystrophy. J Neuropathol Exp Neurol 2002;61:520–530.

39. Schroder R, Mundegar RR, Treusch M, Schlegel U, Blumcke I, Owaribe K, et al. Altered distribution of plectin/hd1 in dystrophinopathies. Eur J Cell Biol 1997;74:165–171.
40. Schroder R, Pacholsky D, Reimann J, Matten J, Wiche G, Furst DO, et al. Primary longitudinal adhesion structures: plectin-containing precursors of costameres in differentiating human skeletal muscle cells. Histochem Cell Biol 2002;118:301–310.
41. Schroder R, Warlo I, Herrmann H, van der Ven PF, Klasen C, Blumcke I, et al. Immunogold EM reveals a close association of plectin and the desmin cytoskeleton in human skeletal muscle. Eur J Cell Biol 1999;78:288–295.
42. Sevcik J, Urbanikova L, Kost'an J, Janda L, Wiche G. Actin-binding domain of mouse plectin. Crystal structure and binding to vimentin. Eur J Biochem 2004;271:1873–1884.
43. Shimizu H, Takizawa Y, Pulkkinen L, Murata S, Kawai M, Hachisuka H, et al. Epidermolysis bullosa simplex associated with muscular dystrophy: phenotype-genotype correlations and review of the literature. J Am Acad Dermatol 1999;41: 950–956.
44. Skalli O, Jones JC, Gagescu R, Goldman RD. Ifap 300 is common to desmosomes and hemidesmosomes and is a possible linker of intermediate filaments to these junctions. J Cell Biol 1994;125:159–170.
45. Smith FD, Eady RAJ, Leigh IM, McMillan JR, Rugg EL, Kelsell DP, et al. Plectin deficiency: hereditary basis for muscular dystrophy with epidermolysis bullosa. Nat Genet 1996;13:450–457.
46. Stegh AH, Herrmann H, Lampel S, Weisenberger D, Andra K, Seper M, et al. Identification of the cytolinker plectin as a major early in vivo substrate for caspase 8 during cd95- and tumor necrosis factor receptor-mediated apoptosis. Mol Cell Biol 2000;20:5665–5679.
47. Takizawa Y, Shimizu H, Rouan F, Kawai M, Udono M, Pulkkinen L, et al. Four novel plectin gene mutations in Japanese patients with epidermolysis bullosa with muscular dystrophy disclosed by heteroduplex scanning and protein truncation tests. J Invest Dermatol 1999;112:109–112.
48. Tanaka H, Hijikata T, Murakami T, Fujimaki N, Ishikawa H. Localization of plectin and other related proteins along the sarcolemma in smooth muscle cells of rat colon. Cell Struct Funct 2001;26:61–70.
49. Vita G, Monici MC, Owaribe K, Messina C. Expression of plectin in muscle fibers with cytoarchitectural abnormalities. Neuromuscul Disord 2003;13:485–492.
50. Wiche G. Role of plectin in cytoskeleton organization and dynamics. J Cell Sci 1998;111:2477–2486.
51. Wiche G, Krepler R, Artlieb U, Pytela R, Aberer W. Identification of plectin in different human cell types and immunolocalization at epithelial basal cell surface membranes. Exp Cell Res 1984;155:43–49.
52. Wiche G, Krepler R, Artlieb U, Pytela R, Denk H. Occurrence and immunolocalization of plectin in tissues. J Cell Biol 1983; 97:887–901.

STEM CELLS
TISSUE-SPECIFIC STEM CELLS

CTACK/CCL27 Accelerates Skin Regeneration via Accumulation of Bone Marrow-Derived Keratinocytes

DAISUKE INOKUMA,[a] RIICHIRO ABE,[a] YASUYUKI FUJITA,[a] MIKAKO SASAKI,[a] AKIHIKO SHIBAKI,[a] HIDEKI NAKAMURA,[a] JAMES R. MCMILLAN,[a] TADAMICHI SHIMIZU,[b] HIROSHI SHIMIZU[a]

[a]Department of Dermatology, Hokkaido University Graduate School of Medicine, Sapporo, Japan; [b]Department of Dermatology, Faculty of Medicine, University of Toyama, Toyama, Japan

Key Words. Bone marrow-derived stem cell • CTACK/CCL27 • CCR10 • Keratinocyte • Wound healing

ABSTRACT

Recent studies have suggested that bone marrow (BM) cells transdifferentiate to regenerate a variety of cellular lineages. Due to the relatively small population of BM-derived cells in each organ, it is still controversial whether these BM-derived cells are really present in sufficient numbers for effective function. Conversely, it is speculated that chemokine/chemokine receptor interactions mediate this migration of the tissue-specific precursor cells from BM into the target tissue. Here, we show that cutaneous T-cell attracting chemokine (CTACK)/CCL27 is the major regulator involved in the migration of keratinocyte precursor cells from BM into skin. By screening various chemokine expression patterns, we demonstrated that CTACK is constitutively expressed in normal skin and upregulated in wounds and that approximately 20% of $CD34^+$ BM cells expressed CCR10, the ligand for CTACK. Intradermal injection of CTACK/CCL27 into the periphery of skin wounds significantly enhanced BM-derived keratinocyte (BMDK) migration, and CTACK/CCL27 neutralizing antibody inhibited this BMDK migration. Furthermore, increased BMDK migration caused by CTACK/CCL27 significantly accelerated the wound-healing process without any influence over either angiogenesis or keratinocyte proliferation. These results provide direct evidence that recruitment of BM keratinocyte precursor cells to the skin is regulated by specific chemokine/chemokine receptor interactions, making possible the development of new regenerative therapeutic strategies. STEM CELLS *2006;24:2810–2816*

INTRODUCTION

Bone marrow (BM)-derived stem cells residing in adult BM possess the unique ability to self-renew and differentiate into multiple cell lineages. A number of recent studies have suggested that BM cells might transdifferentiate and contribute to the regeneration of a variety of nonhematopoietic cell lineages in multiple organs [1–3]. Recent studies have shown that epithelial phenotype BM-derived cells can be found in normal and malignant epithelia without evidence of fusion [4–6] and that cutaneous injury leads to increased engraftment of these BM-derived cells as epidermal cells [7].

Thus far, the concept of BM-derived stem cell plasticity has been cautiously accepted; however, several hurdles remain that have blocked the development of clinical applications. The characteristics of BM-derived stem cells are not fully understood (e.g., the mechanisms causing the tissue-specific migration). Tissue repair and regeneration after injury are thought to involve selective recruitment of circulating or resident stem cell populations [8]. BM-derived, transdifferentiated cells have been detected at the wound site in injured tissues; however, the numbers of these cells are so low that it is impossible to confirm any of their specific biological characteristics or functions.

To increase numbers of BM-derived, transdifferentiated cells, two strategies have been employed. One is to increase the number of BM-derived stem cells present in circulating blood (e.g., using granulocyte colony stimulating factor (G-CSF) to induce mobilization of BM cells [9]) and another is to induce tissue-specific recruitment to increase the final number of BM-derived, transdifferentiated cells in the target tissue (e.g., using stromal cell-derived factor-1α [SDF-1α] to induce homing of hematopoietic stem cells to the BM by binding to CXCR4 [10, 11]). Chemokine/chemokine receptor interactions are thus predicted to play important roles in tissue-specific BM-derived stem cell recruitment.

To further our understanding of the chemokine/chemokine receptor interactions involved in tissue-specific stem cell trafficking, we have investigated the mechanism that controls in vivo migration of BM-derived keratinocyte (BMDK) precursor

Correspondence: Hiroshi Shimizu, M.D., Ph.D., Department of Dermatology, Hokkaido University Graduate School of Medicine, N 15 W 7, Kita-ku, Sapporo 060-8638, Japan. Telephone: +81-11-716-1161, ext. 5962; Fax: +81-11-706-7820; e-mail: Shimizu@med.hokudai.ac.jp Received April 30, 2006; accepted for publication August 14, 2006; first published online in STEM CELLS *EXPRESS* August 24, 2006. 1066-5099/2006/$20.00/0 doi: 10.1634/stemcells.2006-0264

cells into the skin. In addition, to elucidate whether BMDKs have any of the functional roles of keratinocytes, we investigated the contribution of BMDKs to the processes involved in wound healing.

Materials and Methods

Generation of BM-Chimeric Mice

Whole BM cells (5×10^6) from green fluorescent protein (GFP)-transgenic (under control of β-actin promoter) mice (The Jackson Laboratory, Bar Harbor, ME, http://www.jax.org) were transplanted into lethally irradiated (8.5 Gy) wild-type C57BL/6 recipients. Hematopoietic reconstitution was subsequently evaluated in peripheral blood 4 weeks after transplantation.

Wounded and Normal Skin Tissue Preparation

All animal procedures were conducted according to guidelines provided by the Hokkaido University Institutional Animal Care and Use Committee under an approved protocol. We performed skin injury and examined for GFP-expressing cells at least 10 weeks after BM transplantation. The mice were anesthetized, and 6-mm full-thickness punch biopsy wounds were made by folding the back skin. The wounded tissues were subsequently collected after 24 hours in reverse transcription-polymerase chain reaction (RT-PCR) analysis and Western blot analysis or after 3 days in immunofluorescence staining.

RT-PCR Analysis

Total RNA was isolated from normal or wounded skin. RT-PCR analyses of mRNA from chemokines and glyceraldehyde-3-phosphate dehydrogenase (GAPDH) were performed in a thermocycler (GeneAmp PCR system 9600; PerkinElmer Life and Analytical Sciences, Boston, http://www.perkinelmer.com). Primers were as follow: cutaneous T-cell attracting chemokine (CTACK) (sense: 5′-AGCAGCCTCCCGCTGTTACTGTTG-3′, antisense: 5′-TGCTTTATTAGTTTTGCTGTTGGG-3′), mucosae-associated epithelial chemokine (sense: 5′-CATACTTCCCATGGCCTCC-3′, antisense: 5′-GAGAGGCTTCGTGCCTGTG-3′), secondary lymphoid tissue chemokine (SLC) (sense: 5′-ATGGCTCAGATGATGACTCT-3′, antisense: 5′-TACTGGGCTATCCTCTTGA-3′), SDF-1α (sense: 5′-AGTGACGGTAAACCAGTCAG-3′, antisense: 5′-CTTTCTCCAGGTACTCTTGG-3′), macrophage inflammatory protein (MIP)-1α (sense: 5′-AAGGTCTCCACCACTGCCCTTG-3′, antisense: 5′-CTCAGGCATTCAGTTCCAGGTC-3′), MIP-1β (sense: 5′-CCAGCTGTGGTATTCCTGACC-3′, antisense: 5′-AATAGCAGAGTTTCAGCAATGG-3′), MIP-2 (sense: 5′-AGTGAACTGCGCTGTCAATG-3′, antisense: 5′-CTTTGGTTCTTCCGTTGAGG-3′), MIP-3α (sense: 5′-CAAGCGTCTGCTCTTCCTTG-3′, antisense: 5′-TGGATCAGCGCACACAGATT-3′), RANTES (sense: 5′-ATAACGCGTATGCATCACCATATGGCTCGGAC-3′, antisense: 5′-CCAGATCTAGCTCATCTCCAAATAG-3′), TARC (thymus and activation-regulated chemokine) (sense: 5′-AGTGGAGTGTTCCAGGGATG-3′, antisense: 5′-TTTGTGTTCGCCTGTAGTGC-3′), monocyte chemoattractant protein (MCP)-2 (sense: 5′-AGTGCTTCTTTGCCTGCTGCTCATAG-3′, antisense: 5′-ATGAGAAAACACGCAGCCCAGGCACC-3′) MCP-5 (sense: 5′-CTATGCCTCCTGCTCATAGC-3′, antisense: 5′-CTTAACCCACTTCTCCTTGG-3′), TECK (thymus-expressed chemokine) (sense: 5′-CTGGGTTACCAGCACAGGAT-3′, antisense: 5′-CCTCTGGATTCCCACACACT-3′), interferon-γ (IFN-γ) inducible protein-10 (sense: 5′-GGGCCAGTGAGAATGAGGGC-3′, antisense: 5′-TGAGCTAGGGAGGACAAGGAG-3′), MIG (monokine induced by IFN-γ) (sense: 5′-GATCAAACCTGCCTAGATCC-3′, antisense: 5′-GGCTGTGTAGAACACAGAGT-3′), and GAPDH (sense: 5′-GAGGGGCCATCCACAGTCTTC-3′, antisense: 5′-CATCACCATCTTCCAGGAGCG-3′). Aliquots from each amplification reaction were analyzed by electrophoresis in 5% acrylamide-Tris-borate gels.

Western Blot Analysis

Protein lysates from normal and wounded skin tissues were electrophoresed on polyacrylamide gels under reducing conditions and then blotted onto nitrocellulose filters. Filters were blocked with nonfat dried milk and followed by incubation with a primary antibody against SDF-1α (Santa Cruz Biotechnology, Inc., Santa Cruz, CA, http://www.scbt.com), SLC, CTACK, MIP-1α, and MIP-1β (R&D Systems, Inc., Minneapolis, http://www.rndsystems.com). After incubation, the filters were treated with horseradish peroxidase-conjugated anti-rabbit immunoglobulin G, and the resultant immune complexes were visualized.

Immunofluorescence Staining

After 28 days, the wounded tissues were removed. Skin sections were stained with primary antibodies to keratin-14 (Chemicon International, Temecula, CA, http://www.chemicon.com), and the chemokines were used in Western blot analysis. Primary antibodies were visualized using secondary antibodies conjugated to fluorescein isothiocyanate (FITC) or rhodamine isothiocyanate. Fluorescence staining was detected using a confocal laser scanning fluorescence microscope (Laser Scanning Confocal Imaging System MRC 1024; Bio-Rad, Hercules, CA, http://www.bio-rad.com). Keratinocytes expressing both keratin-14 and GFP were presumed to be BMDKs. The number of BMDKs was quantified and calculated as a percentage of the total number of keratinocytes in wounded skin.

Chemokine Receptor Expression in $CD34^+$ BM Cells

BM cells were incubated with FITC-conjugated antibody against CD34 (BD Pharmingen, San Diego, http://www.bdbiosciences.com/pharmingen) and antibodies to CXCR4 (BD Pharmingen), CCR7 (Santa Cruz Biotechnology, Inc.), and CCR10 (Calbiochem, San Diego, http://www.emdbiosciences.com) with secondary PE-conjugated antibodies and then analyzed by flow cytometry (FACScalibur; Becton Dickinson Immunocytometry Systems, San Jose, CA, http://www.bdbiosciences.com).

Migration Assays

Migration assays were performed using Costar Transwell (Corning, Acton, MA, http://www.corning.com) inserts (pore size: 3 μm). Isolated $CD34^+$ BM cells purified by fluorescence-activated cell sorting (FACSVantage; BD Biosciences, San Jose, CA, http://www.bdbiosciences.com) based on surface CD34 staining (>99% purity) were suspended at 1×10^6 cells per milliliter in RPMI 1640 medium containing 0.1% fetal bovine serum. Medium alone or medium containing SDF-1α, SLC, or CTACK (R&D Systems, Inc.) at concentrations of 0, 10, 100, or

500 ng/ml was added to individual lower wells of a 24-well plate. $CD34^+$ BM cells were layered on top of the membrane in the upper chamber of the transwell insert and incubated for 18 hours. For checkerboard analysis, chemokines (100 ng/ml) were added to both the bottom and top chambers. Migration was assessed by counting the cell number in the lower wells. Replicate experiments were performed with separate cultures of cells on separate occasions.

Chemokine Intradermal Injection into the Peripheral Wounded Site

BM-chimeric mice were locally anesthetized and given 4-mm, round skin wounds and received a single intradermal injection of SDF-1α, SLC, or CTACK (1 μg in 30 μl) or phosphate-buffered saline (PBS) (as control) into the peripheral wound sites. After 28 days, the wounded tissue was removed, and the percentage of BMDKs in the wounded skin was calculated.

Neutralizing Antibody Injection into the Wounded Skin

CTACK-neutralizing antibody (0–16 μg in 120 μl) was injected into the periphery of the 4-mm, round wound site, and the percentage of BMDKs in the wounded skin was analyzed as described above.

Mobilization of BM Cells

BM cells of BM-chimeric mice were mobilized into peripheral blood by three daily injections of recombinant mouse G-CSF (TECNE, R&D Systems, Inc.) (150 μg/kg per day). Control mice received a sterile saline solution without G-CSF. Twenty-four hours after the last injection, the mice were given epidermal wounds and received intradermal injections of SDF-1α, SLC, or CTACK (1 μg in 30 μl) or PBS (as control) into their peripheral wounds. Twenty-eight days after wounding, the sites were examined to detect BMDKs as described above.

$CD34^+$ BM Cell Adoptive Transfer

$CD34^+$ BM cells from GFP-transgenic mice were purified using the MACS (magnetic cell sorting) technique (Miltenyi Biotec, Bergisch Gladbach, Germany, http://www.miltenyibiotec.com). Immediately after tail vein injection of $CD34^+$ BM cells (5×10^5 cells/mouse), the mice were given skin wounds and received SDF-1α, SLC, or CTACK (1 μg in 30 μl) or PBS (as control) in their peripheral wound sites. After 28 days of wound healing, BMDKs were counted as described above.

Wound-Healing Analysis

Ten-millimeter, round skin wounds were created, and CTACK (total 3 μg in 100 μl), CTACK-neutralizing antibody (total 16 μg in 100 μl), or PBS (100 μl) (as a control) was injected into the peripheral wound sites. Standardized images of wounds were recorded using a digital camera for analysis of daily wound closure rates.

Analysis of Wound-Healing Angiogenesis

BM-chimeric mice were given 4-mm, round skin wounds and received an intradermal injection of CTACK (1 μg in 30 μl) into the periphery of wounds. After 3 days, the wound sites were removed and skin sections were cut and stained with primary antibodies to CD31 (a marker of endothelial cells) (BD Pharmingen) followed by a secondary antibody conjugated to rhodamine isothiocyanate. The number of capillaries in the dermis of the wounded skin was calculated per surface area or volume of tissue.

Proliferation Assay

Keratinocytes were prepared from the skin of a newborn C57BL/6 mouse. After separation of the epidermis from the dermis with dispase and then 0.5% trypsin, the keratinocytes were cultured in 96-well plates at 1,000 cells in 100 μl of keratinocyte growth medium (Cambrex, East Rutherford, NJ, http://www.cambrex.com) per well. After 24 hours of culture, CTACK was added at concentrations of 1–100 ng/ml. After 72 hours of incubation at 37°C, 10 μl of the tetrazolium salt WST-1 (Dojindo Laboratories, Kumamoto, Japan, http://www.dojindo.co.jp) was added to each well [12]. The plates were incubated for 2 hours at 37°C, and viable cells were determined using a microplate reader at 450 nm with a 630 nm reference wavelength.

In Vitro Keratinocyte Migration Assay

Keratinocytes from C57BL6 mice were cultured in six-well uncoated plates with keratinocyte growth medium until they reached 80% confluency. A cell-free area was created by scraping the keratinocyte monolayer with a plastic pipette tip. Keratinocyte migration to the cell-free area was evaluated after 48 hours of culture in medium alone or medium containing CTACK at concentrations of 0, 1, 10, or 100 ng/ml. The number of migrating keratinocytes was counted in four nonoverlapping fields [13].

RESULTS

BMDKs Were Present in the Basal Layer of the Epidermis

We used a GFP transgenic BM transplantation model. The recipient mice had been lethally and completely irradiated, but to enable their long-term survival, BM was reconstituted from the cells of a donor GFP transgenic mouse. Recruitment of BMDKs to the skin was assessed after the induction of full-thickness wounds. Twenty-eight days after the first incision, the wound was excised and examined for BMDK recruitment. Cells expressing both GFP (a marker of BM origin) and keratin-14 (a marker of basal keratinocyte) were present in the basal layer of the epidermis and were classified as BMDKs (Fig. 1A). Some BM-derived cells are likely to be epidermal Langerhans' cells derived from BM, but the GFP^+ keratin-14^+ cells did not express CD45 (a marker of hematopoietic cells) and CD11c (a marker of Langerhans' cells) (data not shown). Almost all BMDKs were present in the basal layer, but some BMDKs were also present in the bulge region of hair follicles. The percentage of BMDKs as a ratio of all keratinocytes was assessed on three sections from one mouse ($n = 5$). BMDKs were calculated to be present as a total of 0.025% ± 0.009% of all keratinocytes and comprised approximately 0.1% in the basal cell layer.

SDF-1α, SLC, and CTACK Were Expressed in Normal Skin, and CTACK Expression Was Upregulated in Wounded Skin

We therefore supposed that optimum BMDK migration required a higher level of cell recruitment signal generation, such as after

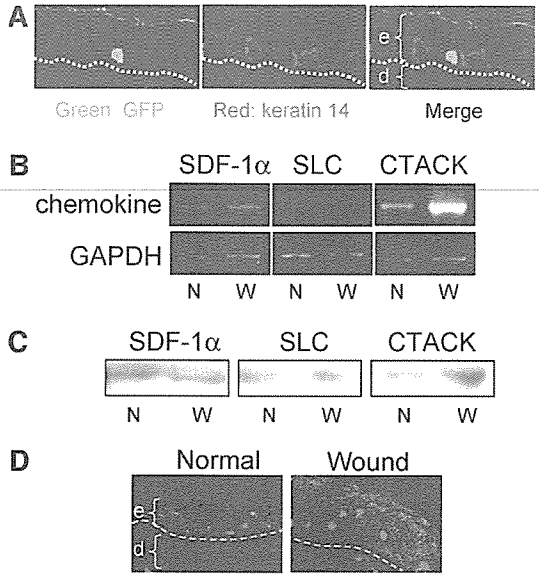

Figure 1. Bone marrow-derived keratinocytes (BMDKs) were identified and CTACK was expressed in wounded skin. **(A):** Engrafted BMDKs in wounded skin expressed both GFP, as a marker of bone marrow origin (green), and keratin-14, as a marker of basal keratinocyte (red), (arrows). **(B–D):** Normal (N) or wounded (W) skin tissue samples were collected and analyzed for chemokine expression as shown in Table 1. The expressions of SDF-1α, SLC, and CTACK were detected by RT-PCR **(B)** and Western blot analysis **(C)** in normal skin and also in skin 24 hours after wounding. These experiments of RT-PCR and Western blot analyses were performed in triplicate. In immunofluorescence staining in the wound edge 3 days after wounding, CTACK expression, in particular, was upregulated (green) **(D)**. SDF-1α and SLC were weakly expressed (data not shown). Nuclei were counterstained with propidium iodide (red). Abbreviations: CTACK, cutaneous T-cell attracting chemokine; d, dermis; e, epidermis; GAPDH, glyceraldehyde-3-phosphate dehydrogenase; GFP, green fluorescent protein; RT-PCR, reverse transcription-polymerase chain reaction; SDF-1α, stromal cell-derived factor-1α; SLC, secondary lymphoid tissue chemokine.

Table 1. Chemokine expression in normal and wounded skin

	RT-PCR		Western blot		IFS	
Wound	**N**	**W**	**N**	**W**	**N**	**W**
SDF	+	+	+	+	+	−
SLC	+	−	+	+	+	−
CTACK	+	+	+	+	+	+
MIP-1α	−	+	−	−	−	−
MIP-1β	−	+	−	−	−	−

MEC (mucosae-associated epithelial chemokine), MIP-2, MIP-3α, RANTES, TARC (thymus and activation regulated chemokine), MCP-2, MCP-5, TECK (thymus-expressed chemokine), IP-10, and MIG (monokine induced by interferon-γ) were not detected. Abbreviations: +, expression; −, no expression; CTACK, cutaneous T-cell attracting chemokine; IFS, immunofluorescence staining; MIP, macrophage inflammatory protein; N, normal skin; RT-PCR, reverse transcription-polymerase chain reaction; SDF, stromal cell-derived factor; SLC, secondary lymphoid tissue chemokine; W, wounded skin.

tissue injury, which could induce a greater accumulation of tissue-specific BM progenitor cells through tissue-specific chemokine/chemokine receptor interactions. To test this possibility in skin, we first examined the expression of a panel of chemokines as possible candidates by RT-PCR, Western blot analysis, and immunofluorescence staining (Table 1). RT-PCR and Western blot analyses were performed with normal skin or with skin 24 hours after wounding, including both epidermis and dermis. Experiments using RT-PCR (Fig. 1B) and Western blot analyses (Fig. 1C) showed that SDF-1α, SLC, and CTACK/CCL27 were constitutively expressed in normal skin and also wounded skin. Only CTACK expression was upregulated in wounded tissue. We examined the location of CTACK expressed in skin. Immunofluorescence staining demonstrated that CTACK expression was upregulated in the epidermis 3 days after wounding (Fig. 1D), whereas SDF-1α and SLC remained only weakly expressed (data not shown). Western blot analysis and immunofluorescence staining showed that MIP-1α and MIP-1β were not detectable, but RT-PCR analysis demonstrated a low level of expression of these chemokines. CTACK has recently been described in mice and humans as being exclusively expressed by keratinocytes [14]. CTACK selectively attracts cutaneous memory T cells [14] by interacting with a specific receptor, CCR10 [15]. CTACK/CCR10 interactions are directly involved in T-cell recruitment to inflamed skin [16]. However, there are no reports that suggest that this interaction is important for other cell types.

CXCR4, CCR7, and CCR10 Expression Were Detected on CD34$^+$ BM Cells

If chemokine/chemokine receptor interactions contribute to the recruitment of BM-derived tissue-specific precursor cells in damaged tissue, a specific chemokine should be upregulated in the target tissue together with a partner receptor expressed on the BM-derived tissue precursor cells. Although the markers identifying keratinocyte precursor cells in BM are still unknown, we chose CD34 as a stem cell marker; CD34 is a known marker for several BM precursor cell populations, including myocytes and neural cells [17, 18]. Expression of CXCR4, CCR7, and CCR10, which are specific receptors for the skin chemokines expressed in wounds (SDF-1α, SLC, and CTACK, respectively), were also analyzed together with CD34$^+$ BM cells using flow cytometry.

Approximately 19.1% of CD34$^+$ BM cells expressed CCR10 (Fig. 2A). In addition, CXCR4 and CCR7 were expressed in 97.4% and 12.9% on the CD34$^+$ cells, respectively (Fig. 2A).

CD34$^+$ BM Cells Migrated in Response to SDF-1α, SLC, and CTACK In Vitro

To confirm that these receptors were actually functional in these cells, in vitro chemotaxis assays were undertaken. CTACK induced CD34$^+$ BM cell migration in a dose-dependent manner (Fig. 2B, 2C). SDF-1α was previously known to induce hematopoietic stem cell migration via CXCR4 interactions [19]. Indeed, SDF-1α enhanced the migration of CD34$^+$ BM cells in a dose-dependent manner (Fig. 2B and data not shown). In addition, SLC enhanced CD34$^+$ BM cell migration (Fig. 2B and data not shown).